Environmental and Experimental Botany 182 (2021): 104302

DOI: https://doi.org/10.1016/j.envexpbot.2020.104302

Sulphur and biothiol metabolism determine toxicity responses and fate of mercury in *Arabidopsis*

Juan Sobrino-Plata*[1(3)], Ángel Barón-Sola*[1], Cristina Ortega-Villasante[1], Víctor Ortega-Campayo[1(4)], Cesar González-Berrocal[1], Carlos Conesa-Quintana[1(4)], Sandra Carrasco-Gil[2(5)], María Muñoz-Pinilla[2], Javier Abadía[2], Ana Álvarez-Fernández[2], Luis E. Hernández[1]

[1]Laboratory of Plant Physiology, Department of Biology, Universidad Autónoma de Madrid, 28049 Madrid, Spain/

[2]Department of Plant Nutrition, Aula Dei Experimental Station-CSIC, 50080 Zaragoza, Spain.

*Authors that contributed equally, and should be considered co-first authors

Corresponding author: Luis E. Hernández
Laboratory of Plant Physiology, Department of Biology,
Universidad Autónoma de Madrid, Campus de Cantoblanco,
Darwin 2, 28049 Madrid, Spain

Current addresses:

[(3)] Departamento de Sistemas y Recursos Naturales, Universidad Politécnica de Madrid, 28040 Madrid, Spain.

[(4)] Centre for Plant Biotechnology and Genomics (CBGP UPM-INIA), Universidad Politécnica de Madrid (UPM) & Instituto Nacional de Investigación y Tecnología Agraria y Alimentaria, Campus de Montegancedo, 28223 Pozuelo de Alarcón, Madrid, Spain

[(5)] Department of Agricultural Chemistry and Food Science, Universidad Autónoma de Madrid, 28049 Madrid, Spain.

Running title: Influence of sulphur metabolism on mercury fate

ABSTRACT

Mercury (Hg) is one of the most hazardous pollutants released by humans and is of global environmental concern. Mercury causes oxidative stress and strong cellular damages in plants, which can be attenuated by the biosynthesis of thiol-rich peptides (biothiols), including glutathione (GSH) and phytochelatins (PCs). We analysed Hg tolerance and speciation in five *Arabidopsis thaliana* genotypes, the wild-type Col-0, three knockdown γ-glutamylcysteine synthetase (γECS) mutants and a knockout PC synthase (PCS) mutant. Mercury-PC complexes were detected in roots by HPLC-ESI-TOFMS, with its abundance being limited in γECS mutants. Analysis of Hg-biothiol complexes in the xylem sap revealed that $HgPC_2$ occurs in wild-type Col-0 *Arabidopsis*, suggesting that Hg could be translocated associated with thiol-rich metabolites. Twenty genes involved in sulphur assimilation, GSH and PCs synthesis were differentially expressed in roots and shoots, implying a complex regulation, possibly involving post-translational mechanisms independent of GSH cellular levels. In summary, the present study describes the importance of biothiol metabolism and adequate GSH levels in Hg tolerance and identifies for the first time Hg-PC complexes in the xylem sap. This finding supports the notion that Hg-biothiol complexes could contribute to Hg mobilisation within plants.

Keywords: plant mercury stress, plant S-assimilation, biothiol dynamics, xylem Hg-PC complexes

1. Introduction

The often indiscriminate use of mercury (Hg) in several human activities, mostly related with chemical industries and gold-mining, and the use of ineffective waste removal practices has caused a progressive contamination of soils and groundwater worldwide (Selin, 2010). Contamination by this hazardous metal needs to be tackled by using costly cleaning approaches that result in numerous environmental side effects (Chaney et al., 1997), whereas plant innate ability to take up metals can be exploited for soil phytoremediation (Krämer, 2005), in a sustainable low cost manner particularly appealing in Hg polluted areas (He et al., 2015). However, this requires tolerant plants able to withstand cellular damages caused by toxic metal(loid)s (Rascio & Navari-Izzo, 2011). Among other mechanisms, Hg and other toxic metal(loid)s activate the rapid synthesis of thiol-rich peptides (biothiols) such as glutathione (GSH; γGlu-Cys-Gly) and phytochelatins (PC; $(\gamma Glu\text{-}Cys)_n$-Gly) where *n* has been reported as being as high as 11, but is generally in the range 2–5 (Cobbett, 2000; Serrano et al., 2015). Biothiols play a critical role in toxic metal tolerance by maintaining the intracellular redox balance and binding toxic metals to form less harmful chemical species (Hernández et al., 2015), which are translocated to vacuoles limiting the cytosolic concentration of free metal (Sharma et al., 2016). Sulphur assimilation and biothiol metabolism are thought to contribute to Hg tolerance and homeostasis (Carrasco-Gil et al., 2011), but there is still limited knowledge on regulatory mechanisms and how those metabolites mitigate Hg-induced stress.

The overall sulphur acquisition and assimilation pathway is highly conserved in the course of evolution starting with sulphate uptake by plant roots, and due to its large reduction energetic costs, it is mostly assimilated in leaves after xylem transport *via*

different classes of sulphate transporters (SULT) (Gigolashvili and Kopriva, 2014). *Arabidopsis* has up to 14 sulphate transporter genes distributed in five groups (*AtSULTR1-5*), with Groups 1 and 2 being more related with S-assimilation (Kopriva, 2006). Once sulphate accumulates, assimilation starts with the synthesis of adenosine phosphosulphate (APS) by adenosine triphosphate sulphurylase (ATPS) from ATP in plastids (see pathway shown in Figs. 6 and 7). APS is reduced subsequently by APS reductase (APR), and then sulphite is reduced by sulphite reductase (SiR). The generated sulfhydryl ion binds to O-acetylserine in a step catalysed by OAS-thiol lyase (OAS-TL), synthesizing cysteine (Cys). This thiol-containing amino acid is then used by the enzyme γ-glutamylcysteine synthetase (γECS), which ligates Cys to glutamate (Glu), to generate γ-glutamylcysteine (γEC). Subsequently, glutathione synthetase (GSH-S) forms GSH from Gly and γEC (Kopriva et al., 2019).

In the present study we evaluate the response of different *Arabidopsis thaliana* genotypes with altered GSH levels under Hg stress, using three γECS mutant alleles *cad2-1*, *pad2-1* and *rax1-1*, which contain limited amounts of GSH relative to the wild type (Col-0) (Parisy et al., 2007), and a *cad1-3* PCS mutant unable to produce PCs (Cobbett, 2000). It is already known that Hg leads to specific stress alterations in biothiol metabolism in comparison with other toxic metals (Sobrino-Plata et al., 2009), but little information is available about its influence on sulphur metabolism. Hence, we analysed the changes in the transcriptional regulation of sulphate uptake and sulphur assimilation pathway under Hg stress. In addition, we determined Cys, Glu-Cys, GSH, and PCs accumulation in roots and shoots to assess plant biothiol distribution. Mercury is taken up by roots where it is strongly retained (Carrasco-Gil et al., 2011, 2013), and only a small portion is thought to be translocated to shoots *via* xylem, as occurs with other metal(loid)s (Khodamoradi et al., 2017); but it may be loaded to the xylem as chelated ions (Álvarez-

Fernández et al., 2014). Here, we analysed xylem sap samples from different *Arabidopsis* genotypes for detection of Hg-biothiol complexes, and we show the presence of $HgPC_2$ complexes in *Arabidopsis* wild type, suggesting that Hg could be transported from the roots to the shoots not only as free ions but also as a biothiol chelated form.

2. Materials and methods

2.1. Plant material, growth conditions and treatments

A. thaliana genotypes used were the wild type Columbia 0 (Col-0), the *cad2-1*, *pad2-1* and *rax1-1* γECS mutants and the *cad1-3* PCS mutant. Seeds were surface-sterilized by agitation in a 15% (v/v) NaClO solution for 10 min, followed by several rinses in distilled sterile water. Seeds were germinated on 0.6 % phytoagar and grown in an Araponics® hydroponic system (Araponics SA, Liège, Belgium). After 4 weeks of growth in a short-day light regime (8 h light / 16 h darkness) at 25 ºC with a modified Hoagland nutrient solution (Tocquin et al., 2003), the nutrient solution was supplemented with 0 or 3 μM $HgCl_2$ and plants were grown for 72 h more. At harvest, shoots and roots were collected separately and stored at -80 ºC until analysis.

2.2. Chlorophyll fluorescence measurements

Chlorophyll (Chl) fluorescence was measured at different light regimes to determine F_o, F_m, $F_{m'}$, F_t, $F_{o'}$, Φ_{PSII}, q_P and NPQ, according to (Maxwell and Johnson, 2000), using a FMS-2 Pulse Modulated Fluorimeter (Hansatech Instruments, Norfolk, UK). Plants were sequentially illuminated with 8000 μmol m^{-2} s^{1} saturating pulses and 400 μmol m^{-2} s^{1} actinic light.

73 *2.3. Mercury and potassium tissue concentration*

74 Organs were dried at 50 ºC for 72 h, milled with mortar and pestle and 100 mg were
75 placed in 4 mL glass vials, and mixed with 1 mL of digestion mixture (HNO_3:H_2O_2:H_2O,
76 0.6:0.4:1 v:v). After vials were securely enclosed with PTFE-stoppers, samples were
77 digested using an autoclave (Presoclave-75 Selecta, Barcelona, Spain) at 120ºC and 1.5
78 atm for 30 min (Ortega-Villasante et al., 2007a). Digests were filtered and diluted in Type
79 I (MiliQ) water to 6 mL, prior to Hg and K concentrations determination using an ICP-
80 MS NexION 300 Perkin-Elmer Sciex (San Jose, CA, USA) equipment.

81 *2.4. Sequencing and alignment of γECS mutants*

82 Genomic DNA was isolated from the shoots of Col-0, *cad2-1*, *pad2-1* and *rax1-1*
83 plants using the DNA Extraction Kit Phytopure (GE Healthcare Life Sciences), and DNA
84 concentration was measured in a NanoDrop® ND-1000 spectrophotometer
85 (Thecnologies Inc., Wilmington, DE, USA). A 637 bp fragment of gene GSH1 (γ-
86 glutamylcysteine synthetase, γ-ECS) was amplified by PCR using primers γECS01F
87 (CGTTCGGATTATTTCTTGGTGT) and γECS02R
88 (GCGGTCCTTGTCAGTGTCTGT), and sequenced in an Applied Biosystems
89 3730/3730xl DNA Sequencer (Foster City, CA, USA). Sequences were revised using the
90 Geneious Pro 5.5.3 software, and compared with GSH1 gene sequence (AT4G23100),
91 and available literature (Supplementary Fig. S1).

92 *2.5. RNA extraction and quantification*

93 Total RNA from shoots and roots of *Arabidopsis* was isolated with TRI Reagent
94 (Ambion, Austin, TX, USA), cleaned using in-column DNAse treatment with the RNeasy
95 Mini Kit (Qiagen, Venlo, Netherlands) (Montero-Palmero et al., 2013), and quantified n
96 a NanoDrop® ND-1000 spectrophotometer (Thecnologies Inc., Wilmington, DE, USA).

RNA integrity was determined with an Agilent 2100 Bioanalyzer equipped with an RNA 6000 Nano LabChip Kit (Agilent Technologies, Santa Clara, CA, USA) using the RNA integrity number (RIN) algorithm of three independent biological replicates (Schroeder et al., 2006), which showed satisfactory RNA quality in all samples, particularly in those prepared from Hg-treated plants (Supplementary Fig. S2).

2.6. Quantitative reverse transcription polymerase chain reaction (qRT-PCR)

Quantitative reverse transcription (RT)-PCR was performed with RNA from *Arabidopsis* shoots and roots in two completely independent biological experiments (three RNA technical replicates each) to synthesize the complementary DNA strand. The RT reaction was performed with random hexamers, using the RETROscript® First Strand Synthesis Kit (Applied Biosystems-Life technologies, Carlsbad, CA, USA). Quantitative PCR was carried out with 50 ng single-stranded cDNA in a final volume of 20 µL, containing 10 µL of SYBR-Green Master Mix (Applied Biosystems-Life Technologies) and 250 nM forward and reverse specific primers (Life Technologies, Supplementary Table 1), using a Real-Time 7000SDS Termocycler (Applied Biosystems-Life Technologies), with denaturation at 95 °C for 10 min, 40 cycles of 15 seconds at 95 °C and 1 min annealing and extension at 60 °C. Gene expression was quantified by using the relative $2^{-\Delta\Delta Ct}$ method (Livak and Schmittgen, 2001), using the glyceraldehyde 3-phosphate dehydrogenase (GAPDH, AT1G13440) gene as internal reference, which showed steady expression under Hg stress (Montero-Palmero et al., 2013).

2.7. Glutathione reductase in gel activity

GR enzymatic activities were determined *in gel* after separation of protein extracts using non-denaturing polyacrylamide electrophoresis (Sobrino-Plata et al., 2009). Protein loading was 20 and 10 µg for shoot and root samples, respectively. The staining solution

was 250 mM Tris-HCl buffer, pH 7.5, supplemented with 0.2 mg mL^{-1} thizolyl blue tetrazolium bromide, 0.2 mg mL^{-1} 2,6-dichlorophenol indophenol, 0.5 mM NADPH and 3.5 mM GSSG.

2.8. Western-blot immunodetection

Immunodetection was performed by Western-blot after denaturing gel electrophoresis (Laemmli, 1970) and blotting onto a nitrocellulose membrane (BioTrace®NT Pall Corporation, East Hills, NY, USA), using a semi-dry procedure (Trans Blot® SD Semi-Dry Electrophoretic Transfer Cell; BioRad, Hercules, CA, USA). Membranes were incubated overnight at 4ºC with the primary antibodies (α-GR (AS06 181) that recognises both plastidial and cytoplasmic isoforms, dil. 1/5000; α–γECS (AS06 186), dil. 1/2500 (Agrisera, Vännäs, Sweden). After incubation with the anti-rabbit secondary antibody linked to horse radish peroxidase (HRP), proteins were detected using the LumiSensor Chemiluminescent HRP Kit (GenScript, Piscataway, NJ, USA), and images were taken with a ChemiDoc™ XRS+ System (BioRad).

2.9. Oxidative stress visualisation by confocal laser scanning microscopy

Col-0 and mutant *Arabidopsis* were germinated for 15 days in Petri dishes filled with solid Murashige-Skoog nutrient solution (containing 1.0% Phytagel, Sigma-Aldrich, San Luis, MI, USA). For oxidative stress staining, seedlings were transferred to a 24-well microtiter plate and immersed in 250 µL of 10 µM 2′,7′-dichlorofluorescein diacetate (H_2DCFDA) solution supplemented with 0 (control) or 3 µM Hg. After 30 min incubation in the darkness, seedlings were briefly counterstained with 25 µM propidium iodide (PI) to visualize cell death, and then samples were observed with a Leica TCS SP2 confocal microscope (Wetzlar, Germany) (Ortega-Villasante et al., 2007).

145 *2.10. Xylem sap extraction and collection*

146 Plants were collected and roots rinsed with distilled water, then excised at the
147 caulinar (floral) stem above the rosette leaves, and the xylem sap was collected directly
148 from the cut with a micropipette. To improve xylem sap exudation in Hg-stressed plants,
149 roots were subjected to external pressure in a portable SKPM 1400 Scholander pressure
150 chamber (SKYE Instruments Ltd., Powys, UK) by applying a 0.3 MPa constant pressure
151 with compressed N_2 gas for less than 20 min. The first 10 µL were discarded to avoid
152 cellular contamination, and the xylem sap collected (45 µL) was transferred to Eppendorf
153 tubes containing 5 µL of acid mixture (10% metaphosphoric acid, 1% formic acid and 10
154 mM EDTA), for preservation of biothiol and biothiol-Hg complexes. Samples were
155 subsequently frozen at -80°C and stored until analysis. Cross-contamination with cellular
156 and phloem exudates was checked routinely by measuring L-malate dehydrogenase (c-
157 MDH) activity (Lopez-Millan et al., 2000) (see Extended Materials and Methods details
158 in Supplementary online material).

159 *2.11. Analysis of biothiols by HPLC-DAD*

160 Biothiols in shoots and roots were analysed by HPLC-UV-diode array detector (DAD)
161 (Sobrino-Plata et al., 2009). Extracts (100 µL) were injected in a Mediterranea SEA18
162 column (5 µm, 250 x 4.6 mm; Teknokroma, San Cugat del Vallés, Spain), using a 1200
163 HPLC system (Agilent, Santa Clara, CA, USA), and biothiols were detected after post-
164 column derivatization with Ellman reagent. Quantification was carried out adding N-
165 acetyl cysteine (N-AcCys; final concentration 250 µM) as internal standard prior to
166 sample homogenization. See full methodology details in the Extended Materials and
167 Methods of Supplementary Material file.

168

169 *2.12. Analysis of biothiols and ascorbate by HPLC-ESI-MS(TOF)*

170 Ascorbate, biothiols and Hg–biothiol complexes were analysed by HPLC-electro
171 spray ionisation (ESI)-time-of-flight mass spectrometry [MS(TOF)], using an HPLC
172 system (Alliance 2795, Waters, Milford, MA, USA), equipped with a reverse-phase
173 monolithic UPLC column (Mediterranea SEA18 3 µm 15 x 0.21 cm, Teknokroma), and
174 coupled to a MS-TOF spectrometer (MicrOTOF, Bruker Daltonics, Bremen, Germany)
175 equipped with an ESI source (Carrasco-Gil *et al.*, 2011), with a mobile phase made with
176 solvents A (0.1% formic acid in miliQ water), and B (0.1% formic acid in acetonitrile)(see
177 Extended Materials and Methods details in Supplementary online material). After
178 chromatographic separation, sample was directed with a flow rate of 200 µL min^{-1} to the
179 ESI interface. The MS(TOF) operated in negative/positive ion mode at -500/4500 V
180 endplate and spray tip voltages, respectively. The orifice voltage was set at 100 V and
181 full scan data acquisition was carried out from *m/z* 50 to1000. The mass axis was
182 calibrated externally using Li-formate adducts (10 mm LiOH, 0.2% (v/v) formic acid and
183 50% (v/v) 2-propanol). The HPLC-ESI-MS(TOF) system was controlled with MicrOTOF
184 Control v.2.2 and HyStar v.3.2, and data were managed with Data Analysis v.3.4
185 (software packages from Bruker Daltonics). Ion chromatograms were extracted with a
186 precision of 0.05 *m/z* units.

187 *2.13. MS/MS for $HgPC_2$ complex analysis*

188 For LC-MS^n (tandem MS spectra) measurements the same HPLC system described
189 above is used, including chromatographic column and analysis conditions, but the MS^n
190 study was performed using a HCT Ultra high-capacity ion trap (Buker Daltonics). ESI
191 conditions were as described previously and to establish the optimum MS^n conditions,
192 standard solutions of $HgPC_2$ were tested. A volume of 20 µL of standard or xylem sap

193 samples was injected into the LC system and MS^n analysis were controlled by HyStar v
194 3.2 software (Bruker Daltonics). MS^n experiments were conducted by selecting the high
195 intensity peak mother ion (740.1 *m/z* for MS, and 536.1 *m/z* for MS^2) at the retention time
196 of the compound chromatographic peak, and data were collected in total ion counting
197 mode, acquiring the spectra in the range 100-1100 *m/z*.

198 *2.14. Statistics*

199 Statistical analysis was performed with SPSS for Windows (v. 19.0), using an
200 ANOVA with Tukey test, with a factorial ANOVA to compare Hg concentration and
201 chlorophyll fluorescence parameters between genotypes and Hg doses. Results shown are
202 means of at least three replicates ± standard deviation, using $p < 0.05$ to detect statistically
203 significant differences.

204 ## 3. Results

205 Biothiol amounts in roots and shoots varied greatly depending on *Arabidopsis*
206 genotypes according to the HPLC-DAD analysis (Fig. 1; Supplementary Table S2).
207 Glutathione was present in all genotypes, but it was at remarkably low concentrations in
208 the γECS mutants *cad2-1*, *pad2-1* and *rax1-1*, when compared with the levels of the wild
209 type Col-0. Due to lack of phenotypic variations, all knock-down mutants were
210 unequivocally identified by PCR amplification and sequence alignment (Supplementary
211 Fig. S1), in agreement with the respective data reported by the labs that isolated those
212 mutants, which express γECS allelic variants with limited catalytic enzymatic activity
213 (Cobbett, 2000; Parisy et al., 2007; Ball et al., 2004). In the phytochelatin-defective
214 mutant *cad1-3*, the GSH concentration in shoots was approximately doubled that found
215 in the wild type. In the presence of 3 μM Hg, PC_2 ((γGlu-Cys)$_2$-Gly), PC_3 ((γGlu-Cys)$_3$-
216 Gly) and PC_4 ((γGlu-Cys)$_4$-Gly) were found in Col-0 roots, whereas only PC_2 and PC_3

accumulated to lesser extent in *rax1-1* roots (Fig. 1; Supplementary Table S2**)**. However, those PCs were barely detected in *cad2-1* and *pad2-1* mutants, and we were unable to quantify them. As expected, we could not detect PCs in *cad1-3* under Hg stress, even though GSH concentrations were the highest observed both in shoots and roots, twice the concentration found in *Arabidopsis* Col-0.

The decrease of GSH levels in *pad2-1*, *cad 2-1* and *rax1-1* and the inability to synthesize PCs in *cad1-3* were accompanied by significant changes in ascorbic acid (ASA), reduced (GSH) and oxidized glutathione (GSSG) concentrations, as measured by HPLC-ESI-MS(TOF) (Table 1). *Arabidopsis* mutants treated with 3 μM Hg had ASA concentrations in roots well above of values found in Col-0, which almost doubled in shoots. On the other hand, GSH concentrations followed the same pattern found using HPLC-DAD, with *pad2-1*, *cad2-1* and *rax1-1* having the lowest values both in roots and shoots, whereas the GSH concentration in *cad1-3* was 2-fold higher than Col-0. Exposure to 3 μM Hg led to general increases in GSH concentrations in shoots and roots of all mutant genotypes, particularly *cad1-3*. With respect to GSSG, concentrations were one order of magnitude lower than those of GSH, but they changed with a similar pattern. As a result, there were minimal changes in the relative content of GSSG irrespective of genotype and occurrence of Hg stress.

The marked changes in ASA and GSH/GSSG contents observed in response to Hg suggested possible alterations in the redox balance of mutant shoots and roots. We firstly analysed the concentrations of Hg in shoots and roots of *Arabidopsis*, which accumulated largely in roots (shoots Hg concentration was less than 1% of that found in roots; Fig. 2a). All γECS mutants had similar Hg levels in roots, which were approximately 50% of the concentration found in Col-0 and *cad1-3* plants (Fig. 2a). However, there were not

significant differences between genotypes but differed in comparison with the control (with $p<0.001$; see Supplementary Table S3). In parallel, we determined photochemical parameters measured by chlorophyll a fluorescence, and observed that there were statistically differences between Hg treatments, *Arabidopsis* genotypes and the interaction of both variable factors (Supplementary Table S3). Non-photochemical quenching (NPQ) was severely impaired in γECS and PCS mutant genotypes both in control and 3 μM Hg-treated plants (Fig. 2b), confirming that limiting biothiols metabolism led to stress in leaves.

The specific inhibition of GR activity is a suitable biomarker of Hg toxicity (Sobrino-Plata et al. 2009), which dropped drastically in roots of GSH depleted mutants *cad2-1*, *pad2-1*, and *rax1-1*, whereas in Col-0 and *cad1-3* roots GR activity was ultimately higher (Fig. 3a). Despite such inhibition, the amount of GR protein did not change appreciably in roots even under Hg-stress independently of the genotype (Fig. 3b). Shoot GR activity only increased slightly in *pad2-1* and *cad1-3* without any substantial alteration in GR amount upon Hg stress (Fig. 3a). On the other hand, shoot γECS protein accumulation clearly diminished in γECS and *cad1-3* mutants under control conditions (40-50% of that found in Col-0), pattern that was also observed under Hg stress in all genotypes (Fig. 3b). However, we could not detect changes in root γECS content among genotypes and Hg treatments, probably due to the low signal obtained by α-γECS immunodetection (high background; Fig. 3b). Redox imbalance associated with GSH depletion was confirmed by using confocal fluorescence microscopy, using H_2DCFDA for oxidative stress staining and IP counterstaining to visualize cell walls and cell death in 15-days old *Arabidopsis* seedlings. Under control conditions, some epidermal cells suffered oxidative stress (yellow arrowheads) probably caused by mechanical damage during manipulation of roots, more clearly observed in the GSH-deficient mutant *pad2-1*

than in Col-0 (Fig. 3c), a symptom that also appeared in previous experiments with alfalfa seedlings (Ortega-Villasante et al., 2005, 2007). H_2DCFDA oxidative stress increased in seedling roots exposed to 3 μM Hg for 30 min, at the time that IP staining of cell damage (pink arrowheads) occurred more clearly at the elongation and apical regions of *pad2-1* than in the wild-type, suggesting an earlier/stronger toxic effect of Hg in the γECS mutant despite individual variation between replicates (Fig. 3c). Similar pattern of Hg-induced damage occurred in *cad2-1* and *rax1-1*, while *cad3-1* was equal to the responses detected in Col-0 seedlings (data not shown). Finally, we confirmed the elevated susceptibility of γECS and PCS mutants to Hg by detecting a drastic drop in root K concentration (Supplementary Fig. S3), crucial macronutrient for plant cell osmotic balance, which was probably caused by loss of membrane integrity and ion leakage occurring upon abiotic stress (Demidchik et al., 2014).

Our preceding study established that the ability of plants to withstand Hg toxicity depends in part on the formation of Hg-PCs complexes, such as $HgPC_2$ ($Hg(\gamma GluCys)_2Gly$) and $HgPC_3$ ($Hg(\gamma GluCys)_3Gly$) (Carrasco-Gil et al., 2011). Full HPLC-ESI-MS(TOF) analysis of biothiol ligands and Hg-biothiol complexes (Hg-PCs) in shoots and roots of showed clear differences between all studied *Arabidopsis* genotypes (Fig. 4). In shoots, we could only detect free PC_2 ($[PC_2\text{-}H]^-$; *m/z* 538.1) and PC_3 ($[PC_3\text{-}H]^-$; *m/z* 770.2) ligands, whereas in roots there were oxidized variants of free PCs, such as ($[PC_3oxd\text{-}H]^-$; *m/z* 768.2), Hg-PC complexes like $HgPC_2$ ($[HgPC_2\text{-}H]^-$; *m/z* 738.1) and $HgPC_3$ ($[HgPC_3\text{-}H]^-$; *m/z* 970.1). The graphical table included in Fig. 4b shows the groups of free ligands, oxidised PCs and Hg-biothiol complexes, found in shoots and roots of all *Arabidopsis* genotypes. The results in *rax1-1* and *cad2-1* roots closely resembled those found for Col-0, where we detected $[HgPC_2\text{-}H]^-$ and $[HgPC_3\text{-}H]^-$, albeit with a rather weak signal (data not shown). On the other hand, in *pad2-1* we only found GSH

([GSH+H]$^+$; *m/z* 308.1) and GSSG ([GSSG+H]$^+$; *m/z* 613.3) in roots and shoots, which were better detected in positive mode, in addition to PC_2, that was just over the background signal. As expected, *cad1-3* did not accumulate free PCs or Hg-PCs complexes.

Recent studies indicated that toxic elements (Cd and As) are chelated with PCs in roots impeding translocation to shoots and potentially helping plants to attenuate stress, in a manner that metal(loid)-PCs complexes would accumulate in root vacuoles (Liu et al., 2010; Mendoza-Cózatl et al., 2008). However, to some extent metal(loid)s may travel to shoots bound to organic ligands such as PCs (Shi et al., 2019). To determine whether Hg had a similar behaviour, we studied the possible occurrence of biothiols and Hg-PCs complexes in xylem sap by HPLC-ESI-MS(TOF) using both positive and negative modes. Since Hg blocks water movement through plant vascular tissues, we used a Scholander pressure chamber to apply a pneumatic pressure to allow xylem sap to flow from the cut stem. Similarly, Hg almost blocked completely the xylem water flow in pea plants, whereas in Cd-treated plants root pressure sufficed to collect several µLs of xylem sap (Belimov et al., 2015). To prevent cross-contamination of phloem and broken cells fluids, particularly when relatively high pneumatic pressure was used, MDH activity was measured routinely in all xylem sap samples. Data shown in Supplementary Fig. S4 suggest that cross-contamination was negligible in three xylem sap samples obtained from *Arabidopsis* Col-0 treated with 3 µM Hg. The compounds GSH ([GSH+H]$^+$; *m/z* 308.1) and GSSG ([GSSG+H]$^+$; *m/z* 613.3) appeared in the xylem sap of all genotypes, albeit signals were lower in γECS mutants (data not shown). The characteristic PC_2 peak ([PC_2+H]$^+$; *m/z* 540.1) appeared in xylem sap of Col-0 and, at very low intensity, also in *rax1-1* (Fig. 5). This compound coeluted with another of *m/z* 538.1, which was tentatively

identified as oxidized PC_2 (PC_2oxd). However, PC_2 or PC_2oxd were not detected in *cad2-1*, *pad2-1* and, as expected, PCS mutant *cad1-3*.

To confirm the nature of PC_2oxd we run in parallel a hydroponic experiment with Col-0 *Arabidopsis* treated with 10 μM Cd for 72 h. In this case, we got a better signal in MS(TOF) in negative mode with a *m/z* 536.1 ($[PC_2oxd\text{-}H]^-$) (Supplementary Fig. S5a); molecular ion that was subjected to tandem MS ($-MS^2$), and was compared with those obtained using PC_2 (*m/z* 538.13) and PC_2oxd (*m/z* 536.1) standards, which had characteristic daughter ions at *m/z* 254.1 and 128.0 (Supplementary Fig. S5c). Incidentally, we were unable to observe any Cd-PC complex, in spite of using ESI-MS(TOF) settings appropriate for detection of $CdPC_2$, as we obtained the characteristic peaks associated with the natural Cd isotopic distribution (major $[CdPC_2\text{-}H]^-$ peak at *m/z* 650.0) by direct injection of a Cd:PC_2 standard (Supplementary Fig. S5b).

In Col-0 xylem sap, along with to PC_2 and PC_2oxd we found only a compound with the characteristic Hg-isotopic fingerprint that could correspond to Hg-PCs complexes, which was tentatively assigned to $HgPC_2$, eluting separately from free biothiol ligands (Fig. 5a). The MS(TOF) spectrum (in positive mode) of the detected compound ($[HgPC_2+H]^+$; *m/z* 740.1) fitted well with theoretical data and also with a Hg:PC_2 standard mixture (1:1) (Fig. 5b). The identity of the *m/z* 740.1 ion peak of Col-0 xylem samples was confirmed using tandem MS/MS analysis. The same Hg:PC_2 standard mixture was used to set up analytical conditions, and the *m/z* 740.1 mother ion was selected and sent to the collision cell for fragmentation (MS^2). Several major daughter ions appeared with *m/z* 609.1, 536.1 and 508.1 both in the $HgPC_2$ standard and the Col-0 xylem sap (Fig. 5c). Some of these ions were tentatively identified by comparing with those detected in Hg-biothiol complexes analysis as follows: *m/z* 609.1 was assigned to $[HgPC_2\text{-}Glu]^+$; *m/z*

536.1 matched $[PC_2oxd\text{-}2H]^+$, and *m/z* 508.1 was assigned to $[HgGSH+H]^+$. Further identification of the *m/z* 536.1 ion, with the highest intensity peak, was obtained after a second fragmentation (MS^3) resulting in various ions. The MS^3 spectra of both the xylem sap and the standard mixture were also very similar, with a major *m/z* 507.1 daughter ion (possibly $[GSH-H]^+$), with a second *m/z* 489.1 ion also present in both samples (Fig. 5d). Therefore, we can assert that $HgPC_2$ complexes could be transferred from roots to shoots *via* xylem flux, process that did not occur in *rax1-1*, *cad2-1* and *cad1-3* mutants. Nevertheless, we could not determine to what extent Hg flows to shoots via xylem, since our ICP-MS analysis failed to detect Hg above background levels, probably due to the small volume of sample collected (10-50 μL).

In view of the relevant role that biothiol metabolism has in tolerance to and speciation of Hg in plants, we analysed the expression pattern of 20 genes involved in sulphur uptake, assimilation and incorporation to biothiols under Hg-stress (Gigolashvili and Kopriva, 2014). The expression pattern was organ-dependent, with some genes being over-expressed in the shoots of certain mutants treated with Hg (Fig. 6), whereas in the roots we only detected gene down-regulation under Hg stress (Fig. 7). Regarding transcription factors in shoots, *MYB28* was induced only in the γECS-mutants *cad2-1* and *pad2-1* under Hg exposure, whereas *MYB51* was suppressed in *rax1-1*. On the other hand, both *MYB28* and *MYB51* were down-regulated in roots under Hg-stress, especially in *rax1-1* and *cad1-3* mutants (Fig. 7). We also found significant down-regulation of SLIM1 in roots of all mutant *Arabidopsis* genotypes (Fig. 7; Supplementary Tables S4 and S5).

Among the genes involved in sulphur incorporation and assimilation in shoots, the sulphur transporter *SULTR1;2* had the highest over-expression in Hg-treated *cad2-1*, *rax1-1* and *cad1-3* plants, whereas a strong repression was observed in Col-0 (Fig. 6;

Suppl. Table S4). A similar repression appeared in Col-0 for ATP sulphurylase (*ATPS3*) and APS reductase (*APR1* and *APR3*) (Fig. 6). On the other hand, *ATPS4* (only in *pad2-1*), *APR1*, *APR2* and *APR3* (only in *rax1-1*), were over-expressed in *pad2-1*, *rax1-1* and *cad1-3* plants treated with 3 μM Hg. With regard to GSH and PCs metabolism, we only observed a minor down-regulation under Hg stress, particularly significant for *cad2-1* and *pad2-1* O-acetylserine (thiol) lyase (*OASTLA* and *OASTLB*) genes. Interestingly, expression of the phytochelatin synthase genes *PCS1* and *PC2* decreased in leaves in Hg-treated plants, being particularly significant in *pad2-1*, *rax1-1* and *cad 1-3* (Fig. 6, Suppl. Table S4). Finally, in roots under Hg stress we only observed significant gene down-regulation, mostly in the mutant genotypes. Especially relevant was the down-regulation of sulphate transporters, including a remarkable decrease for *SULTR1;2* in *cad2-1*, *rax1-1* and *cad1-3* (Fig. 7). The expression of other sulphur transporters decreased, including that of *SULTR2;1* in *rax1-1* and *cad1-3*, and *SULTR3;5*, which was very intense in all Hg-exposed *Arabidopsis* genotypes. With regard to sulphur assimilation genes, the most consistent changes occurred in *cad1-3*, where *ATPS1*, *ATPS3*, *SiR*, *OASTLB*, *OASTLC*, *γECS*, *GSH-S*, *PCS1* and *PCS2* expression decreased in plants treated with 3 μM Hg (Fig. 7, Suppl. Table S5).

4. Discussion

Knock-down of γECS drastically decreased biothiol concentrations under control and Hg-stress conditions, particularly in the *cad2-1* and *pad2-1* mutants (Fig. 1), confirming previous results in these GSH-depleted genotypes (Parisy et al., 2007; Ball et al., 2004; Cobbett, 2000), and in *Arabidopsis* leaf discs and plants treated with similar doses of Hg and Cd (Sobrino-Plata et al., 2014a; 2014b). Interestingly, the mildly-affected knock-down *rax1-1* γECS mutant exposed to 3 μM Hg also accumulated PC_2 and PC_3

(but not PC_4) in roots, but to a lower extent than did wild-type plants as observed in Cd-treated plants (Sobrino-Plata et al., 2014b). We were unable to detect PCs in shoots, organs that accumulated much less Hg than roots (by two orders of magnitude), since a certain Hg concentration threshold may be required to trigger synthesis of PCs. In fact, numerous PCs appeared in Col-0 and *rax1-1* leaf discs subjected to direct infiltration with 3 and 30 μM Hg; behaviour that was accentuated at longer exposure times (48 h) when PC_2 and PC_3 also appeared in *cad2-1* (Sobrino-Plata et al., 2014a). On the other hand, the inability to synthesize PCs in *cad1-3* led to a significantly higher GSH accumulation in when compared to Col-0 (Fig. 1, Table 1). Interestingly, this increase became larger under Hg stress, in agreement with our previous observations in *cad1-3* leaf discs infiltrated with 3 μM Hg for 24 h (Sobrino-Plata et al., 2014a). It has been proposed recently that PCS functions as a transpeptidase important for GSH and conjugated GSH turnover, which may explain the high GSH levels found in *cad1-3* plants (Kühnlenz et al., 2015).

Depletion of GSH elicited a severe oxidative stress and enhanced cell death pattern with 3 μM Hg in *pad2-1*, resembling the patchy pattern that occurred under acute Hg stress in alfalfa seedlings that probably depends on the specific physiological status of each epidermal cell (Ortega-Villasante et al., 2007, 2005). Mercury stress also caused a marked inhibition of GR activity in the roots of γECS mutants in comparison with Col-0 and *cad1-3*, without any changes in enzyme amount. The mutant *cad1-3* lacked the ability to form Hg-PC complexes, but the Hg-induced damage was similar to that found in Col-0, possibly due to enhanced GSH levels in this mutant. Strong GR inhibition occurred in roots of *cad2-1*, *pad2-1* and *rax1-1* treated with 10 μM Hg for 72 h, which also suffered extensive alterations in membrane proteins (i.e., degradation of H^+-ATPase and strong inhibition of NADPH-oxidase; Sobrino-Plata et al., 2014b). Such alteration of membrane integrity would lead to ion leakage, which could explain low root K concentrations under

412 Hg stress, particularly in γECS and PCS *Arabidopsis* mutants (Suppl. Fig. S3). Our results
413 are thus comparable to the strong effects of Hg toxicity on K concentration observed in
414 wheat (Sahu et al., 2012) and *Brassica juncea* (Wang et al., 2018) plants. Potassium is
415 important for tolerance to various abiotic and biotic stresses, with a critical role in the
416 osmotic and water balance of plant cells (Srivastava et al., 2020), which seem to be
417 hampered by Hg particularly in GSH depleted *Arabidopsis* plants.

418 The GR inhibition appears to be triggered specifically by Hg over certain
419 concentrations in *Medicago sativa* or *Silene vulgaris*, whereas other toxic elements
420 usually lead to an enhanced activity (Sobrino-Plata et al., 2013; 2009), as can be used as
421 a marker of Hg-stress. Paradoxically, besides the strong GR inhibition there were minor
422 and non-consistent changes in the proportion of GSSG in the analysed *Arabidopsis*
423 genotypes (Table 1), even though insufficient effective GR decreases the GSH/GSSG
424 ratio (Müller-Schüssele et al., 2020). However, our results concurs with the minimal
425 oxidation of homoglutathione (hGSH) (less than 15%) found in extremely damaged
426 alfalfa seedlings treated with 30 μM Hg (Ortega-Villasante et al., 2007). It is possible that
427 even though GSH synthesis was compromised in γECS mutants, much severe and chronic
428 cellular damage would be required to observe relevant GSH oxidation in roots. In addition,
429 alternative pathways to maintain GSH cellular levels under Hg stress may operate: Recent
430 evidence suggest that methylglyoxal (MG), an ubiquitous toxic sub-product of carbon
431 metabolism and lipid peroxidation that accumulates remarkably under plant abiotic stress,
432 is detoxified with the sequential action of glyoxalase I (lactoylglutathione lyase) and
433 glyoxalase II (hydroxyacylglutathione hydrolase) to generate GSH (Hoque et al., 2016).
434 Incidentally, oxidative stress caused by Cd and Se in *Lepidium sativum* plants was
435 associated with a strong accumulation of MG and other 2-oxoaldehydes (Gómez-Ojeda

et al., 2013). Hence, elucidating whether this alternative stress response pathway operates also under Hg stress should be the matter of future experiments.

The poorer tolerance to Hg caused by limited GSH also led to alterations of chlorophyll fluorescence parameters, with a remarkable NPQ decrease (Fig. 2), in accordance with results obtained in *Arabidopsis* treated with Hg, Cd and Cu over 72 h (Maksymiec et al., 2007; Sobrino-Plata et al., 2014a). Alteration of GSH levels in γECS and PCS mutants decreased NPQ, observed even at control conditions, was also reported previously under metal stress in those *Arabidopsis* genotypes (Aranjuelo et al., 2014; Larsson et al., 2001). GSH plays a central role in chloroplast redox balance, keeping ASA and xanthophyll pools reduced at optimal levels to sustain NPQ under stress (Yin et al., 2010), which may be hampered in γECS mutants, or affected by excess GSH cellular concentration in *cad1-3*. Incidentally, transgenic tobacco plants engineered to overproduce GSH (2-fold increase than wild type plants) suffered stronger oxidative damage under high light stress in parallel with strong inhibition of photosynthesis (Creissen et al., 1999). On the other hand, the increase in ASA shoot concentrations under Hg stress was particularly intense in γECS mutant genotypes. Similar response was found in Cd-treated *cad2-1* mutants, where ASA concentration was higher than in wild-type plants (Jozefczak et al., 2015). In this respect, recent experiments showed that increases in ASA concentrations are a common response of plants to metal stress, especially in shoots where this antioxidant metabolite helps protecting the photosynthetic apparatus, which may be hampered by both the lack of GSH and the oxidative stress induced by Hg (Bielen et al., 2013). This damage could explain the diminution of the plastidial γECS content in shoots that appeared in *Arabidopsis* mutants even under control conditions, alteration that also appeared under Hg stress in all genotypes (Fig. 3b). The observed increase in ASA concentration under limited GSH concentration may be a general

461 mechanism of ASA-GSH redox cycle acclimation, as was found in genetically engineered
462 *Physcomitrella patens* with diminished functional GR and enhanced GSH oxidation
463 subjected to high light stress (Müller-Schüssele et al., 2020).

464 Mercury is thought to bind strongly to cell walls of epidermal and vascular cells of
465 the root, possibly bound to the Cys thiol residues of proteins, thus preventing translocation
466 to shoots (Carrasco-Gil et al., 2011; 2013), as found in roots of different plant species
467 (Carrasco-Gil et al., 2011; Sobrino-Plata et al., 2009; 2013; 2014b). Interestingly, γECS
468 mutants roots had significant lower Hg concentration than Col-0, with no effects in shoots,
469 whereas stronger Hg-induced damages appeared in the mutants. Similarly, metal
470 accumulation in shoots did not change in Cd- and Hg-treated *cad2-1* plants (Li et al.,
471 2006), in line with the view that cellular biothiol levels have little impact on overall plant
472 metal distribution (Lee et al., 2003). On the other hand, it is known that transpiration is
473 strongly impaired by Hg (Moreno et al., 2008), a toxic metal that drastically reduces
474 metabolic-driven water conductance in roots (Lovisolo et al., 2008). Interestingly, short-
475 term exposure of pea plants to 2 μM Hg led to drastic diminution of xylem flow (Belimov
476 et al., 2015). This could also be related with the strong diminution of K concentration in
477 roots, specifically in γECS *Arabidopsis* mutants, caused by 3 μM Hg; being K an
478 important macronutrient for ionic and water plant homeostasis (Srivastava et al., 2020).
479 Therefore, it is feasible that the strong Hg-stress in γECS mutants caused poorer water
480 flow to shoot, which impelled us to use the Scholander pressure chamber to collect
481 enough xylem sap. Ultimately, this toxic effect would also limit Hg and K uptake and
482 translocation to the aerial part of Hg-exposed plants.

483 Xylem conforms, along with phloem, the major long-distance transport system for
484 movement and distribution of water, ions and metals throughout the plant (Álvarez-

485 Fernández et al., 2014). Cadmium transport by the xylem determines Cd accumulation in
486 shoots, which depends on loading driven by metal transporters (Wu et al., 2015), while
487 biothiols have been suggested as long distance carriers for Cd in the phloem of *Brassica*
488 *napus* (Mendoza-Cózatl et al., 2008). The high stability of Hg-PC complexes found in
489 plant roots could provide a basis for Hg long-distance transport, as it was suggested by
490 the association of Hg with sulphur in stems and leaf veins of alfalfa plants exposed to Hg
491 (Carrasco-Gil et al., 2013). HPLC-ESI-MS(TOF) analysis revealed for the first time that
492 $[HgPC_2\text{-}H]^+$ indeed occurs in the xylem sap of Col-0 (Fig. 5), identity that was confirmed
493 by MS^n analysis, with daughter molecular ions in the MS^2 and MS^3 spectra matching
494 those of standards. We also detected free $[PC_2\text{-}H]^-$ and $[PC_2oxd\text{-}H]^-$ in xylem sap,
495 confirming our preliminary findings in the xylem sap of Col-0 plants treated with 10 μM
496 Cd for 72 h (Supplementary Fig. 2). Oxidised PC_2 was also found in the xylem sap of
497 *Brassica napus* plants subjected to Cd (Mendoza-Cózatl et al., 2008) and *Arabidopsis*
498 seedlings treated with As (Liu et al., 2010), but metal(loid)-PC complexes were not found
499 in those cases. Moreover, a very low concentration of As was found in xylem sap of the
500 metallophyte castor bean, which was accompanied again with oxidised GSH and PC_2 (Ye
501 et al., 2010), probably as a result of the oxidative stress and redox imbalance triggered by
502 metal(loid)s. As(III)- and Cd-biothiols complexes may be less stable than those formed
503 with Hg in our conditions, able to withstand even acidic extraction. Nevertheless, future
504 research effort should be aimed to characterise the mechanism that controls xylem loading
505 of Hg-PC complexes, which will probably require highly sensitive and spatially resolved
506 analytical techniques.

507 Plants treated with metals experience alterations in sulphate uptake and assimilation
508 (Na & Salt, 2011; Nocito et al., 2006), which prompted us to analyse the expression of
509 twenty genes involved in the sulphur assimilatory pathway under Hg-stress. Our results

510 revealed in all *A. thaliana* genotypes tested different responses to Hg in roots and shoots,
511 indicating that both organs had independent stress responses as found with other metals
512 (Jozefczak et al., 2014). In general, we observed a modest response of genes with fold-
513 changes generally not larger than three (significant at $p < 0.05$), following the same
514 pattern of recent transcriptomic analyses performed after short-term Hg treatments in
515 *Medicago* (Montero-Palmero et al., 2013; Zhou et al., 2013), barley (Lopes et al., 2013),
516 rice (Chen et al., 2014) and tomato (Hou et al., 2015).

517 With regard to sulphur metabolism regulation, several transcription factors have
518 been reported to be overexpressed under S-starvation, such as the central hub SLIM1
519 regulator and several R2R3-MYBs, including MYB28 and MYB51 (Frerigmann and
520 Gigolashvili, 2014). However, we only observed MYB28 upregulation in *cad2-1* and
521 *pad2-1* shoots under Hg stress. Incidentally, a rice R2R3-MYB (OsARM1) has been
522 found to be upregulated in stems and leaves upon As exposure (Wang et al., 2017), and
523 several R2R3-MYBs control response to Cd-stress *via* ABA signalling (Zhang et al.,
524 2019). However, we found marked MYB28, MYB51 and SLIM1 down-regulation in
525 roots of Hg-stressed γECS and *cad1-3 Arabidopsis* mutants, which can likely explain the
526 low expression of several sulphur assimilatory pathway genes. Little is known about how
527 SLIM1 may operate under abiotic stress, which may undergo post-transcriptional redox
528 imbalance regulation occurring in Hg-treated γECS mutants (Koprivova and Kopriva,
529 2014).

530 Sulphate uptake is a bottleneck in plant sulphur incorporation, which were
531 upregulated under metal stress, such as *SULTR1;1* in roots of maize (Nocito et al., 2006)
532 and *Arabidopsis* (Ferri et al., 2017). However, other members of the SULTR transporter
533 gene family in Chinese cabbage plantlets and sorghum responded in different manner in

leaves and roots under metal stresses (Shahbaz et al., 2014; Akbudak, Filiz, & Kontbay, 2018). We found that sulphate transporter *SULTR1;2* was up-regulated in shoots in *Arabidopsis* γECS and PCS mutants under Hg-stress, response was also found for *SULTR3;5* in roots of *Medicago* just after 6 h exposure to 3 μM Hg (Montero-Palmero et al., 2013). Conversely, *SULTR1;2* was down-regulated in shoots of Col-0 and roots of all *Arabidopsis* mutants, following the same pattern of *SULTR2;1* and *SULTR3;5* (Figs. 6, 7), in agreement with the short-term down regulation of *SULTR3;3* in rice seedlings treated with 25 μM Hg for 3 h (Chen et al., 2014). Cadmium exposure and sulphate limitation revealed differences in the transcriptional control of three sulphate transporter (*SULTR1;2*) genes in *Brassica juncea* (Lancilli et al., 2014). Similarly, *SULTR1* and *SULTR2* expression decreased in roots and shoots of Cd-treated *Arabidopsis* at high Cd doses (over 40 μM) (Yamaguchi et al., 2016). Therefore, *SULTR* expression under metal stress changed depending on the plant organ, supplied metal and doses, implying a complex regulation and specific responses. Time-course experiments to monitor the metal induced expression of *SULTR1;2* showed that in roots it peaked a few hours after metal exposure but subsided subsequently (Jobe et al., 2012). It is feasible that the GSH depletion promoted *SULTR1;2* expression in shoots under Hg stress, where we observed significant redox alterations, whereas under acute cellular damage there might be a general transcriptional down-regulation in roots (Montero-Palmero et al., 2013).

APRs are key enzymes of sulphur assimilatory pathway, that produce sulphite from adenosine 5′ phosphosulphate (Kopriva, 2006), genes that were up-regulated in *Arabidopsis* γECS and PCS mutants shoots treated with Hg, in agreement with the overexpression found in short-term Hg-treated *Medicago* (Montero-Palmero et al., 2013). However, the rest of S-assimilatory pathway genes in shoots and roots of γECS and PCS

mutants were modestly affected or down-regulated by Hg (Figs. 6, 7). It must be emphasized that until now none of the transcriptomic analyses carried out in plants treated with Hg showed significant changes in gene expression of enzymes involved in Cys, γEC, GSH or PCs synthesis (Chen et al., 2014; Hou et al., 2015; Lopes et al., 2013; Montero-Palmero et al., 2013; Zhou et al., 2013). In consequence, despite the several significant changes in S-assimilatory gene expression, occurring mainly in GSH deprived plants, we cannot rule out that the process can be post-transcriptionally controlled. Several stress hormones and the redox cellular balance can contribute to altered enzymatic activities that modify biothiol pools (Kopriva et al., 2019); mechanisms that should be the matter of future research.

5. Conclusions

Depletion of GSH led to stronger Hg toxicity visualised by strong inhibition of GR activity, a poor accumulation of Hg-PC complexes and a limited translocation of $HgPC_2$ to shoots via xylem transport. Despite GR inhibition, the proportion of GSSG did not increase consistently with Hg-induced damage, which may imply the activation of alternative pathways to maintain GSH cellular pool, such as the methylglyoxal detoxification. Sulphur metabolism and accumulation of biothiols help withstanding Hg-induced oxidative stress, but the mechanisms of regulation remain to be characterised in detail. Although some responses at the transcriptional level were detected, we cannot rule out post-transcriptional regulation, which probably play a relevant role to procure sufficient biothiols to limit Hg induced damage. In this sense, transcriptional sulphur-assimilation regulation could be independent of GSH cellular levels, in spite of being an essential factor to maintain the cellular redox balance that was compromised by Hg.

Supplementary information file

Supplementary information contains extended Materials and Methods, alignment of γECS gene sequences of *Arabidopsis thaliana* genotypes used in our study, quality of RNA extracted from samples under Hg stress, concentration of K, MDH activity as a cytosolic contamination test in xylem sap, HPLC-ESI-TOFMS analysis of *Arabidopsis* treated with Cd, primers for qPCR analysis, concentration of biothiols in the different Arabidopsis genotypes exposed to Hg, factorial ANOVA data of photochemical parameters, and qRT-PCR expression values of selected genes of sulphur metabolism.

Acknowledgments

Work supported by the Spanish State Research Agency (AEI) co-financed with the European Regional Development Fund (FEDER) (projects AGL2014-53771-R and AGL2017-87591-R to LEH and AGL2016-75226-R to AAF and JA; AEI/FEDER, UE). We thank Dr. M. Isabel Orús (Dept. Biology UAM, Madrid, Spain) for help in using the Scholander pressure chamber for obtaining xylem samples.

References

Akbudak, M.A., Filiz, E., Kontbay, K., 2018. Genome-wide identification and cadmium induced expression profiling of sulfate transporter (*SULTR*) genes in sorghum (Sorghum bicolor L.). BioMetals. https://doi.org/10.1007/s10534-017-0071-5

Alvarez-Fernández, A., Díaz-Benito, P., Abadía, A., López-Millán, A.-F., Abadía, J., 2014. Metal species involved in long distance metal transport in plants. Front. Plant Sci. https://doi.org/10.3389/fpls.2014.00105

Álvarez-Fernández, A., Díaz-Benito, P., Abadía, A., López Millán, A.F., Abadía, J., 2014. Metal species involved in long distance metal transport in plants. Front. Plant Sci. https://doi.org/10.3389/fpls.2014.00105

Aranjuelo, I., Doustaly, F., Cela, J., Porcel, R., Müller, M., Aroca, R., Munné-Bosch, S.,

607 Bourguignon, J., 2014. Glutathione and transpiration as key factors conditioning
608 oxidative stress in *Arabidopsis thaliana* exposed to uranium. Planta 239, 817–830.
609 https://doi.org/10.1007/s00425-013-2014-x

610 Ball, L., Accotto, G.P., Bechtold, U., Creissen, G., Funck, D., Jimenez, A., Kular, B.,
611 Leyland, N., Mejia-Carranza, J., Reynolds, H., Karpinski, S., Mullineaux, P.M.,
612 2004. Evidence for a direct link between glutathione biosynthesis and stress
613 defense gene expression in *Arabidopsis*. Plant Cell 16, 2448–2462.
614 https://doi.org/10.1105/tpc.104.022608

615 Belimov, A.A., Dodd, I.C., Safronova, V.I., Malkov, N. V., Davies, W.J., Tikhonovich,
616 I.A., 2015. The cadmium-tolerant pea (*Pisum sativum* L.) mutant SGECdt is more
617 sensitive to mercury: Assessing plant water relations. J. Exp. Bot. 66, 2359–2369.
618 https://doi.org/10.1093/jxb/eru536

619 Bielen, A., Remans, T., Vangronsveld, J., Cuypers, A., 2013. The influence of metal
620 stress on the availability and redox state of ascorbate, and possible interference
621 with its cellular functions. Int. J. Mol. Sci. 14, 6382–6413.
622 https://doi.org/10.3390/ijms14036382

623 Carrasco-Gil, S., Alvarez-Fernández, A., Sobrino-Plata, J., Millán, R., Carpena-Ruiz,
624 R.O., Leduc, D.L., Andrews, J.C., Abadía, J., Hernández, L.E., 2011.
625 Complexation of Hg with phytochelatins is important for plant Hg tolerance. Plant.
626 Cell Environ. 34, 778–791. https://doi.org/10.1111/j.1365-3040.2011.02281.x

627 Carrasco-Gil, S., Siebner, H., LeDuc, D.L., Webb, S.M., Millán, R., Andrews, J.C.,
628 Hernández, L.E., 2013. Mercury localization and speciation in plants grown
629 hydroponically or in a natural environment. Environ. Sci. Technol. 47, 3082–3090.

630 Chaney, R.L., Malik, M., Li, Y.M., Brown, S.L., Brewer, E.P., Angle, J.S., Baker,
631 A.J.M., 1997. Phytoremediation of soil metals. Curr. Opin. Biotechnol.
632 https://doi.org/10.1016/S0958-1669(97)80004-3

633 Chang, S., Wei, F., Yang, Y., Wang, A., Jin, Z., Li, J., He, Y., Shu, H., 2015.
634 Engineering tobacco to remove mercury from polluted soil. Appl. Biochem.
635 Biotechnol. https://doi.org/10.1007/s12010-015-1549-7

636 Chen, Y.A., Chi, W.C., Trinh, N.N., Huang, L.Y., Chen, Y.C., Cheng, K.T., Huang,
637 T.L., Lin, C.Y., Huang, H.J., 2014. Transcriptome profiling and physiological
638 studies reveal a major role for aromatic amino acids in mercury stress tolerance in
639 rice seedlings. PLoS One 9, 1–11. https://doi.org/10.1371/journal.pone.0095163

640 Cobbett, C.S., 2000. Phytochelatins and their roles in heavy metal detoxification. Plant
641 Physiol. https://doi.org/10.1104/pp.123.3.825

642 Cobbett, C.S., May, M.J., Howden, R., Rolls, B., 1998. The glutathione-deficient,
643 cadmium-sensitive mutant, *cad2-1*, of *Arabidopsis thaliana* is deficient in γ-
644 glutamylcysteine synthetase. Plant J. 16, 73–78. https://doi.org/10.1046/j.1365-
645 313x.1998.00262.x

646 Creissen, G., Firmin, J., Fryer, M., Kular, B., Leyland, N., Reynolds, H., Pastori, G.,
647 Wellburn, F., Baker, N., Wellburn, A., Mullineaux, P., 1999. Elevated glutathione
648 biosynthetic capacity in the chloroplasts of transgenic tobacco plants paradoxically
649 causes increased oxidative stress. Plant Cell 11, 1277–1291.
650 https://doi.org/doi.org/10.1105/tpc.11.7.1277

651 Cunningham, S.D., Ow, D.W., 1996. Promises and prospects of phytoremediation. Plant
652 Physiol. https://doi.org/10.1104/pp.110.3.715

653 Demidchik, V., Straltsova, D., Medvedev, S.S., Pozhvanov, G.A., Sokolik, A., Yurin,
654 V., 2014. Stress-induced electrolyte leakage: the role of K^+-permeable channels
655 and involvement in programmed cell death and metabolic adjustment. J. Exp. Bot.
656 65, 1259–1270. https://doi.org/10.1093/jxb/eru004

657 Domínguez-Solís, J.R., Gutiérrez-Alcalá, G., Romero, L.C., Gotor, C., 2001. The
658 cytosolic O-acetylserine(thiol)lyase gene is regulated by heavy metals and can
659 function in cadmium tolerance. J. Biol. Chem.
660 https://doi.org/10.1074/jbc.M009574200

661 Emamverdian, A., Ding, Y., Mokhberdoran, F., Xie, Y., 2015. Heavy metal stress and
662 some mechanisms of plant defense response. Sci. World J.
663 https://doi.org/10.1155/2015/756120

664 Ernst, W.H.O., Krauss, G.J., Verkleij, J.A.C., Wesenberg, D., 2008. Interaction of

heavy metals with the sulphur metabolism in angiosperms from an ecological point of view. Plant, Cell Environ. https://doi.org/10.1111/j.1365-3040.2007.01746.x

Ferri, A., Lancilli, C., Maghrebi, M., Lucchini, G., Sacchi, G.A., Nocito, F.F., 2017. The sulfate supply maximizing *Arabidopsis* shoot growth is higher under long- than short-term exposure to cadmium. Front. Plant Sci. 8, 854. https://doi.org/10.3389/fpls.2017.00854

Frerigmann, H., Gigolashvili, T., 2014. Update on the role of R2R3-MYBs in the regulation of glucosinolates upon sulfur deficiency. Front. Plant Sci. https://doi.org/10.3389/fpls.2014.00626

Gigolashvili, T., Kopriva, S., 2014. Transporters in plant sulfur metabolism. Front. Plant Sci. https://doi.org/10.3389/fpls.2014.00442

Gómez-Ojeda, A., Corrales-Escobosa, A.R., Wrobel, Kazimierz, Yanez-Barrientos, E., Wrobel, Katarzyna, 2013. Effect of Cd(II) and Se(IV) exposure on cellular distribution of both elements and concentration levels of glyoxal and methylglyoxal in *Lepidium sativum*. Metallomics 5, 1254–1261. https://doi.org/10.1039/c3mt00058c

Gworek, B., Bemowska-Kałabun, O., Kijeńska, M., Wrzosek-Jakubowska, J., 2016. Mercury in marine and oceanic waters—A review. Water. Air. Soil Pollut. 227. https://doi.org/10.1007/s11270-016-3060-3

Harmens, H., Den Hartog, P.R., Ten Bookum, W.M., Verkleij, J.A.C., 1993. Increased zinc tolerance in *Silene vulgaris* (Moench) Garcke is not due to increased production of phytochelatins. Plant Physiol. 103, 1305–1309. https://doi.org/10.1104/pp.103.4.1305

He, F., Gao, J., Pierce, E., Strong, P.J., Wang, H., Liang, L., 2015. In situ remediation technologies for mercury-contaminated soil. Environ. Sci. Pollut. Res. https://doi.org/10.1007/s11356-015-4316-y

Heiss, S., Schäfer, H.J., Haag-Kerwer, A., Rausch, T., 1999. Cloning sulfur assimilation genes of *Brassica juncea* L.: Cadmium differentially affects the expression of a putative low-affinity sulfate transporter and isoforms of ATP sulfurylase and APS

694 reductase. Plant Mol. Biol. https://doi.org/10.1023/A:1006169717355

695 Hernández, L.E., Sobrino-Plata, J., Montero-Palmero, M.B., Carrasco-Gil, S., Flores-
696 Cáceres, M.L., Ortega-Villasante, C., Escobar, C., 2015. Contribution of
697 glutathione to the control of cellular redox homeostasis under toxic metal and
698 metalloid stress. J. Exp. Bot. https://doi.org/10.1093/jxb/erv063

699 Hoque, T.S., Hossain, M.A., Mostofa, M.G., Burritt, D.J., Fujita, M., Tran, L.S.P.,
700 2016. Methylglyoxal: An emerging signaling molecule in plant abiotic stress
701 responses and tolerance. Front. Plant Sci. 7, 1–11.
702 https://doi.org/10.3389/fpls.2016.01341

703 Hou, J., Liu, X., Wang, J., Zhao, S., Cui, B., 2015. Microarray-based analysis of gene
704 expression in *Lycopersicon esculentum* seedling roots in response to cadmium,
705 chromium, mercury, and lead. Environ. Sci. Technol. 49, 1834–1841.
706 https://doi.org/10.1021/es504154y

707 Jobe, T.O., Sung, D.Y., Akmakjian, G., Pham, A., Komives, E.A., Mendoza-Cózatl,
708 D.G., Schroeder, J.I., 2012. Feedback inhibition by thiols outranks glutathione
709 depletion: A luciferase-based screen reveals glutathione-deficient γ-ECS and
710 glutathione synthetase mutants impaired in cadmium-induced sulfate assimilation.
711 Plant J. 70, 783–795. https://doi.org/10.1111/j.1365-313X.2012.04924.x

712 Jozefczak, M., Bohler, S., Schat, H., Horemans, N., Guisez, Y., Remans, T.,
713 Vangronsveld, J., Cuypers, A., 2015. Both the concentration and redox state of
714 glutathione and ascorbate influence the sensitivity of *Arabidopsis* to cadmium.
715 Ann. Bot. https://doi.org/10.1093/aob/mcv075

716 Jozefczak, M., Keunen, E., Schat, H., Bliek, M., Hernández, L.E., Carleer, R., Remans,
717 T., Bohler, S., Vangronsveld, J., Cuypers, A., 2014. Differential response of
718 *Arabidopsis* leaves and roots to cadmium: Glutathione-related chelating capacity
719 vs antioxidant capacity. Plant Physiol. Biochem. 83, 1–9.
720 https://doi.org/10.1016/j.plaphy.2014.07.001

721 Khodamoradi, K., Khoshgoftarmanesh, A.H., Maibody, S.A.M.M., 2017. Root uptake
722 and xylem transport of cadmium in wheat and triticale as affected by exogenous
723 amino acids. Crop Pasture Sci. https://doi.org/10.1071/CP17061

724 Kopriva, S., 2006. Regulation of sulfate assimilation in *Arabidopsis* and beyond. Ann.
725 Bot. https://doi.org/10.1093/aob/mcl006

726 Kopriva, S., Malagoli, M., Takahashi, H., 2019. Sulfur nutrition: Impacts on plant
727 development, metabolism, and stress responses. J. Exp. Bot.
728 https://doi.org/10.1093/jxb/erz319

729 Kopriva, S., Mugford, S.G., Baraniecka, P., Lee, B.-R., Matthewman, C.A., Koprivova,
730 A., 2012. Control of sulfur partitioning between primary and secondary
731 metabolism in *Arabidopsis*. Front. Plant Sci.
732 https://doi.org/10.3389/fpls.2012.00163

733 Koprivova, A., Kopriva, S., 2014. Molecular mechanisms of regulation of sulfate
734 assimilation: First steps on a long road. Front. Plant Sci.
735 https://doi.org/10.3389/fpls.2014.00589

736 Krämer, U., 2005. Phytoremediation: Novel approaches to cleaning up polluted soils.
737 Curr. Opin. Biotechnol. https://doi.org/10.1016/j.copbio.2005.02.006

738 Kühnlenz, T., Westphal, L., Schmidt, H., Scheel, D., Clemens, S., 2015. Expression of
739 *Caenorhabditis elegans* PCS in the AtPCS1-deficient *Arabidopsis thaliana cad1-3*
740 mutant separates the metal tolerance and non-host resistance functions of
741 phytochelatin synthases. Plant Cell Environ. https://doi.org/10.1111/pce.12534

742 Laemmli, U.K., 1970. Cleavage of structural proteins during the assembly of the head
743 of bacteriophage T4. Nature. https://doi.org/10.1038/227680a0

744 Lancilli, C., Giacomini, B., Lucchini, G., Davidian, J.C., Cocucci, M., Sacchi, G.A.,
745 Nocito, F.F., 2014. Cadmium exposure and sulfate limitation reveal differences in
746 the transcriptional control of three sulfate transporter (*Sultr1;2*) genes in *Brassica*
747 *juncea*. BMC Plant Biol. https://doi.org/10.1186/1471-2229-14-132

748 Larsson, E.H., Bornman, J.F., Asp, H., 2001. Physiological effects of cadmium and UV-
749 B radiation in phytochelatin-deficient *Arabidopsis thaliana*, *cad1-3*. Aust. J. Plant
750 Physiol. 28, 505–512. https://doi.org/10.1071/PP01067

751 Lee, S., Petros, D., Moon, J.S., Ko, T.S., Goldsbrough, P.B., Korban, S.S., 2003. Higher

752 levels of ectopic expression of *Arabidopsis* phytochelatin synthase do not lead to
753 increased cadmium tolerance and accumulation. Plant Physiol. Biochem. 41, 903–
754 910. https://doi.org/10.1016/S0981-9428(03)00140-2

755 Li, Y., Dankher, O.P., Carreira, L., Smith, A.P., Meagher, R.B., 2006. The shoot-
756 specific expression of γ-glutamylcysteine synthetase directs the long-distance
757 transport of thiol-peptides to roots conferring tolerance to mercury and arsenic.
758 Plant Physiol. 141, 288–298. https://doi.org/10.1104/pp.105.074815.levels

759 Liu, W.J., Wood, B.A., Raab, A., McGrath, S.P., Zhao, F.J., Feldmann, J., 2010.
760 Complexation of arsenite with phytochelatins reduces arsenite efflux and
761 translocation from roots to shoots in *Arabidopsis*. Plant Physiol.
762 https://doi.org/10.1104/pp.109.150862

763 Livak, K.J., Schmittgen, T.D., 2001. Analysis of relative gene expression data using
764 real-time quantitative PCR and the $2^{-\Delta\Delta CT}$ method. Methods.
765 https://doi.org/10.1006/meth.2001.1262

766 Lopes, M.S., Iglesia-Turiño, S., Cabrera-Bosquet, L., Serret, M.D., Bort, J., Febrero, A.,
767 Araus, J.L., 2013. Molecular and physiological mechanisms associated with root
768 exposure to mercury in barley. Metallomics. https://doi.org/10.1039/c3mt00084b

769 Lopez-Millan, A.F., Morales, F., Abadia, A., Abadia, J., 2000. Effects of iron
770 deficiency on the composition of the leaf apoplastic fluid and xylem sap in sugar
771 beet. Implications for iron and carbon transport. Plant Physiol. 124, 873–884.
772 https://doi.org/10.1104/pp.124.2.873

773 Lovisolo, C., Tramontini, S., Flexas, J., Schubert, A., 2008. Mercurial inhibition of root
774 hydraulic conductance in *Vitis* spp. rootstocks under water stress. Environ. Exp.
775 Bot. https://doi.org/10.1016/j.envexpbot.2007.11.005

776 Maksymiec, W., Wójcik, M., Krupa, Z., 2007. Variation in oxidative stress and
777 photochemical activity in *Arabidopsis thaliana* leaves subjected to cadmium and
778 excess copper in the presence or absence of jasmonate and ascorbate. Chemosphere
779 66, 421–427. https://doi.org/10.1016/j.chemosphere.2006.06.025

780 Marrugo-Negrete, J., Marrugo-Madrid, S., Pinedo-Hernández, J., Durango-Hernández,

J., Díez, S., 2016. Screening of native plant species for phytoremediation potential at a Hg-contaminated mining site. Sci. Total Environ. 542, 809–816. https://doi.org/10.1016/j.scitotenv.2015.10.117

Maxwell, K., Johnson, G.N., 2000. Chlorophyll fluorescence - A practical guide. J. Exp. Bot. https://doi.org/10.1093/jxb/51.345.659

Mendoza-Cózatl, D.G., Butko, E., Springer, F., Torpey, J.W., Komives, E.A., Kehr, J., Schroeder, J.I., 2008. Identification of high levels of phytochelatins, glutathione and cadmium in the phloem sap of *Brassica napus*. A role for thiol-peptides in the long-distance transport of cadmium and the effect of cadmium on iron translocation. Plant J. 54, 249–259. https://doi.org/10.1111/j.1365-313X.2008.03410.x

Montero-Palmero, M.B., Martín-Barranco, A., Escobar, C., Hernández, L.E., 2014. Early transcriptional responses to mercury: A role for ethylene in mercury-induced stress. New Phytol. 201, 116–130. https://doi.org/10.1111/nph.12486

Moreno, F.N., Anderson, C.W.N., Stewart, R.B., Robinson, B.H., 2008. Phytofiltration of mercury-contaminated water: Volatilisation and plant-accumulation aspects. Environ. Exp. Bot. https://doi.org/10.1016/j.envexpbot.2007.07.007

Müller-Schüssele, S.J., Wang, R., Gütle, D.D., Romer, J., Rodriguez-Franco, M., Scholz, M., Buchert, F., Lüth, V.M., Kopriva, S., Dörmann, P., Schwarzländer, M., Reski, R., Hippler, M., Meyer, A.J., 2020. Chloroplasts require glutathione reductase to balance reactive oxygen species and maintain efficient photosynthesis. Plant J. 103, 1140–1154. https://doi.org/10.1111/tpj.14791

Mustroph, A., Barding, G.A., Kaiser, K.A., Larive, C.K., Bailey-Serres, J., 2014. Characterization of distinct root and shoot responses to low-oxygen stress in *Arabidopsis* with a focus on primary C- and N-metabolism. Plant, Cell Environ. https://doi.org/10.1111/pce.12282

Na, G.N., Salt, D.E., 2011. The role of sulfur assimilation and sulfur-containing compounds in trace element homeostasis in plants. Environ. Exp. Bot. 72, 18–25. https://doi.org/10.1016/j.envexpbot.2010.04.004

Nagajyoti, P.C., Lee, K.D., Sreekanth, T.V.M., 2010. Heavy metals, occurrence and toxicity for plants: A review. Environ. Chem. Lett. https://doi.org/10.1007/s10311-010-0297-8

Nocito, F.F., Lancilli, C., Crema, B., Fourcroy, P., Davidian, J.-C., Sacchi, G.A., 2006. Heavy metal stress and sulfate uptake in maize roots. Plant Physiol. https://doi.org/10.1104/pp.105.076240

Nocito, F.F., Pirovano, L., Cocucci, M., Sacchi, G.A., 2002. Cadmium-induced sulfate uptake in maize roots. Plant Physiol. https://doi.org/10.1104/pp.002659

Ortega-Villasante, C., Hernández, L.E., Rellán-Alvarez, R., Del Campo, F.F., Carpena-Ruiz, R.O., 2007. Rapid alteration of cellular redox homeostasis upon exposure to cadmium and mercury in alfalfa seedlings. New Phytol. 176, 96–107. https://doi.org/10.1111/j.1469-8137.2007.02162.x

Ortega-Villasante, C., Rellán-Álvarez, R., Del Campo, F.F., Carpena-Ruiz, R.O., Hernández, L.E., 2005. Cellular damage induced by cadmium and mercury in *Medicago sativa*. J. Exp. Bot. 56, 2239–2251. https://doi.org/10.1093/jxb/eri223

Page, V., Feller, U., 2015. Heavy metals in crop plants: transport and redistribution processes on the whole plant level. Agronomy. https://doi.org/10.3390/agronomy5030447

Parisy, V., Poinssot, B., Owsianowski, L., Buchala, A., Glazebrook, J., Mauch, F., 2007. Identification of PAD2 as a γ-glutamylcysteine synthetase highlights the importance of glutathione in disease resistance of *Arabidopsis*. Plant J. https://doi.org/10.1111/j.1365-313X.2006.02938.x

Ping Li, Feng, X., Shang, L., Qiu, G., Meng, B., Liang, P., Zhang, H., 2008. Mercury pollution from artisanal mercury mining in Tongren, Guizhou, China. Appl. Geochemistry. https://doi.org/10.1016/j.apgeochem.2008.04.020

Rascio, N., Navari-Izzo, F., 2011. Heavy metal hyperaccumulating plants: How and why do they do it? And what makes them so interesting? Plant Sci. 180, 169–181. https://doi.org/10.1016/j.plantsci.2010.08.016

838 Rellan-Alvarez, R., Ortega-Villasante, C., Alvarez-Fernandez, A., del Campo, F.F.,
839 Hernandez, L.E., 2006. Stress responses of *Zea mays* to cadmium and mercury.
840 Plant Soil. https://doi.org/10.1007/s11104-005-3900-1

841 Ruiz, O.N., Daniell, H., 2009. Genetic engineering to enhance mercury
842 phytoremediation. Curr. Opin. Biotechnol.
843 https://doi.org/10.1016/j.copbio.2009.02.010

844 Sahu, G.K., Upadhyay, S., Sahoo, B.B., 2012. Mercury induced phytotoxicity and
845 oxidative stress in wheat (*Triticum aestivum* L.) plants. Physiol. Mol. Biol. Plants
846 18, 21–31. https://doi.org/10.1007/s12298-011-0090-6

847 Schroeder, A., Mueller, O., Stocker, S., Salowsky, R., Leiber, M., Gassmann, M.,
848 Lightfoot, S., Menzel, W., Granzow, M., Ragg, T., 2006. The RIN: An RNA
849 integrity number for assigning integrity values to RNA measurements. BMC Mol.
850 Biol. https://doi.org/10.1186/1471-2199-7-3

851 Schützendübel, A., Polle, A., 2002. Plant responses to abiotic stresses: Heavy metal-
852 induced oxidative stress and protection by mycorrhization. J. Exp. Bot. 53, 1351–
853 1365. https://doi.org/10.1093/jxb/53.372.1351

854 Selin, N.E., 2009. Global biogeochemical cycling of mercury: A review. Annu. Rev.
855 Environ. Resour. 34, 43–63.
856 https://doi.org/10.1146/annurev.environ.051308.084314

857 Serrano, N., Díaz-Cruz, J.M., Ariño, C., Esteban, M., 2015. Recent contributions to the
858 study of phytochelatins with an analytical approach. TrAC - Trends Anal. Chem.
859 https://doi.org/10.1016/j.trac.2015.04.031

860 Sharma, P., Jha, A.B., Dubey, R.S., Pessarakli, M., 2012. Reactive oxygen species,
861 oxidative damage, and antioxidative defense mechanism in plants under stressful
862 conditions. J. Bot. 2012, 1–26. https://doi.org/10.1155/2012/217037

863 Sharma, S.S., Dietz, K.J., Mimura, T., 2016. Vacuolar compartmentalization as
864 indispensable component of heavy metal detoxification in plants. Plant Cell
865 Environ. https://doi.org/10.1111/pce.12706

Shi, W., Zhang, Y., Chen, S., Polle, A., Rennenberg, H., Luo, Z. Bin, 2019. Physiological and molecular mechanisms of heavy metal accumulation in nonmycorrhizal versus mycorrhizal plants. Plant Cell Environ. https://doi.org/10.1111/pce.13471

Sobrino-Plata, J., Carrasco-Gil, S., Abadía, J., Escobar, C., Álvarez-Fernández, A., Hernández, L.E., 2014a. The role of glutathione in mercury tolerance resembles its function under cadmium stress in *Arabidopsis*. Metallomics 6, 356–366.

Sobrino-Plata, J., Meyssen, D., Cuypers, A., Escobar, C., Hernández, L.E., 2014b. Glutathione is a key antioxidant metabolite to cope with mercury and cadmium stress. Plant Soil 1–13.

Sobrino-Plata, J., Herrero, J., Carrasco-Gil, S., Pérez-Sanz, A., Lobo, C., Escobar, C., Millán, R., Hernández, L.E., 2013. Specific stress responses to cadmium, arsenic and mercury appear in the metallophyte *Silene vulgaris* when grown hydroponically. RSC Adv. 3, 4736–4744.

Sobrino-Plata, J., Ortega-Villasante, C., Laura Flores-Cáceres, M., Escobar, C., Del Campo, F.F., Hernández, L.E., 2009. Differential alterations of antioxidant defenses as bioindicators of mercury and cadmium toxicity in alfalfa. Chemosphere 77, 946–954.

Srivastava, A.K., Shankar, A., Chandran, A.K.N., Sharma, M., Jung, K.H., Suprasanna, P., Pandey, G.K., Foyer, C., 2020. Emerging concepts of potassium homeostasis in plants. J. Exp. Bot. 71, 608–619. https://doi.org/10.1093/jxb/erz458

Takahashi, H., Kopriva, S., Giordano, M., Saito, K., Hell, R., 2011. Sulfur assimilation in photosynthetic organisms: Molecular functions and regulations of transporters and assimilatory enzymes. Annu. Rev. Plant Biol. https://doi.org/10.1146/annurev-arplant-042110-103921

Tocquin, P., Corbesier, L., Havelange, A., Pieltain, A., Kurtem, E., Bernier, G., Perilleux, C., 2003. A novel high efficiency, low maintenance, hydroponic system for synchronous growth and flowering of *Arabidopsis thaliana*. BMC Plant Biol.

Turnbull, C.G.N., Lopez-Cobollo, R.M., 2013. Heavy traffic in the fast lane: Long-

distance signalling by macromolecules. New Phytol. https://doi.org/10.1111/nph.12167

Viehweger, K., 2014. How plants cope with heavy metals. Bot. Stud. https://doi.org/10.1186/1999-3110-55-35

Wang, F.Z., Chen, M.X., Yu, L.J., Xie, L.J., Yuan, L.B., Qi, H., Xiao, M., Guo, W., Chen, Z., Yi, K., Zhang, J., Qiu, R., Shu, W., Xiao, S., Chen, Q.F., 2017. OsARM1, an R2R3 MYB Transcription factor, is involved in regulation of the response to arsenic stress in rice. Front. Plant Sci. https://doi.org/10.3389/fpls.2017.01868

Wang, J., Anderson, C.W.N., Xing, Y., Fan, Y., Xia, J., Shaheen, S.M., Rinklebe, J., Feng, X., 2018. Thiosulphate-induced phytoextraction of mercury in *Brassica juncea*: Spectroscopic investigations to define a mechanism for Hg uptake. Environ. Pollut. 242, 986–993. https://doi.org/10.1016/j.envpol.2018.07.065

Wong, C.K.E., Cobbett, C.S., 2009. HMA P-type ATPases are the major mechanism for root-to-shoot Cd translocation in *Arabidopsis thaliana*. New Phytol. 181, 71–78. https://doi.org/10.1111/j.1469-8137.2008.02638.x

Wu, Z., Zhao, X., Sun, X., Tan, Q., Tang, Y., Nie, Z., Hu, C., 2015. Xylem transport and gene expression play decisive roles in cadmium accumulation in shoots of two oilseed rape cultivars (*Brassica napus*). Chemosphere. https://doi.org/10.1016/j.chemosphere.2014.09.099

Yamaguchi, C., Takimoto, Y., Ohkama-Ohtsu, N., Hokura, A., Shinano, T., Nakamura, T., Suyama, A., Maruyama-Nakashita, A., 2016. Effects of cadmium treatment on the uptake and translocation of sulfate in *Arabidopsis thaliana*. Plant Cell Physiol. https://doi.org/10.1093/pcp/pcw156

Ye, W.L., Wood, B.A., Stroud, J.L., Andralojc, P.J., Raab, A., McGrath, S.P., Feldmann, J., Zhao, F.J., 2010. Arsenic speciation in phloem and xylem exudates of castor bean. Plant Physiol. https://doi.org/10.1104/pp.110.163261

Yin, Y., Li, S., Liao, W., Lu, Q., Wen, X., Lu, C., 2010. Photosystem II photochemistry, photoinhibition, and the xanthophyll cycle in heat-stressed rice leaves. J. Plant

924 Physiol. https://doi.org/10.1016/j.jplph.2009.12.021

925 Zhang, P., Wang, R., Ju, Q., Li, W., Tran, L.S.P., Xu, J., 2019. The R2R3-MYB
926 transcription factor MYB49 regulates cadmium accumulation. Plant Physiol.
927 https://doi.org/10.1104/pp.18.01380

928 Zhou, Z.S., Yang, S.N., Li, H., Zhu, C.C., Liu, Z.P., Yang, Z.M., 2013. Molecular
929 dissection of mercury-responsive transcriptome and sense/antisense genes in
930 *Medicago truncatula*. J. Hazard. Mater. 252–253, 123–131.
931 https://doi.org/10.1016/j.jhazmat.2013.02.011

932

Table 1. Concentration of ascorbic acid (ASA), reduced (GSH) and oxidized (GSSG) glutathione (in nmol g^{-1} FW) measured by HPLC-ESI-TOFMS, and glutathione redox ratio %GSSG [GSSG/(GSH + GSSG)] x 100] in wild type (Col-0), *cad2-1*, *pad2-1*, *rax1-1* and *cad1-3 Arabidopsis thaliana* treated with 0 and 3 µM Hg for 72 h. Different letters in the same column denote significant differences between treatments and genotypes at $p < 0.05$ (n = 4)

			ASA	GSH	GSSG	%GSSG
SHOOTS	Control	**Col-0**	$4777.77^{a} \pm 286.32$	$284.33^{a} \pm 27.35$	$6.63^{a} \pm 2.16$	2.3
		cad2-1	$5897.23^{a} \pm 1719.75$	$37.12^{b} \pm 14.31$	$1.22^{c} \pm 0.31$	3.2
		pad2-1	$5413.97^{a} \pm 840.92$	$13.49^{b} \pm 3.62$	$0.87^{c} \pm 0.37$	6.0
		rax1-1	$5472.31^{a} \pm 663.86$	$55.41^{b} \pm 3.55$	$3.66^{b} \pm 0.56$	6.2
		cad1-3	$4595.73^{a} \pm 291.22$	$312.09^{a} \pm 32.47$	$6.10^{a} \pm 1.18$	1.9
	3 µM Hg	**Col-0**	$6232.62^{a} \pm 1890.08$	$281.16^{a} \pm 43.41$	$9.25^{a} \pm 1.33$	3.2
		cad2-1	$11718.71^{b} \pm 1650.06$	$51.41^{b} \pm 18.09$	$1.67^{c} \pm 0.34$	3.1
		pad2-1	$11882.27^{b} \pm 1126.86$	$21.08^{b} \pm 5.80$	$1.37^{c} \pm 0.82$	6.1
		rax1-1	$10728.59^{b} \pm 1149.24$	$145.62^{c} \pm 26.91$	$6.65^{a} \pm 1.48$	4.4
		cad1-3	$10399.66^{b} \pm 1413.69$	$406.59^{d} \pm 32.64$	$12.83^{b} \pm 1.50$	3.1
ROOTS	Control	**Col-0**	$1388.48^{a} \pm 256.64$	$195.78^{a} \pm 34.61$	$7.40^{a} \pm 0.99$	3.6
		cad2-1	$1336.04^{a} \pm 49.52$	$44.62^{cd} \pm 10.28$	$1.99^{c} \pm 0.61$	4.3
		pad2-1	$1357.04^{a} \pm 260.35$	$14.09^{d} \pm 1.65$	$0.93^{c} \pm 0.33$	6.2
		rax1-1	$1302.52^{a} \pm 25.00$	$55.38^{c} \pm 3.49$	$3.71^{bc} \pm 1.48$	6.3
		cad1-3	$1553.45^{b} \pm 62.04$	$280.14^{ab} \pm 5.50$	$11.19^{b} \pm 0.88$	3.8
	3 µM Hg	**Col-0**	$1276.32^{a} \pm 225.05$	$145.56^{a} \pm 7.44$	$4.24^{a} \pm 0.99$	2.8
		cad2-1	$1796.90^{b} \pm 194.19$	$82.48^{c} \pm 30.96$	$2.91^{ab} \pm 0.23$	3.4
		pad2-1	$1707.96^{b} \pm 125.50$	$63.68^{c} \pm 11.38$	$2.92^{ab} \pm 0.60$	4.4
		rax1-1	$1924.59^{b} \pm 92.65$	$170.52^{d} \pm 18.48$	$6.84^{a} \pm 1.52$	3.9
		cad1-3	$1474.29^{ab} \pm 129.65$	$513.82^{b} \pm 46.85$	$25.03^{d} \pm 0.34$	4.6

Fig.1 Summary of HPLC analysis of biothiol concentrations in shoots and roots (in $nmol \cdot g^{-1}$ FW) in wild type (Col-0), *cad2-1*, *pad2-1*, *rax1-1* and *cad1-3 Arabidopsis thaliana* treated with 0 and 3 μM Hg for 72 h. Different biothiols are represented by spheres with different colours, with sphere diameters proportional to concentrations found. The concentration-to-volume scale is represented by the grey spheres at the bottom. Note that PC_2 were detected in roots of *cad2-1* and *pad2-1* treated with 3 μM Hg. but could not be quantified. For statistics and complete description of concentration values, please see Supplementary Table S2.

Fig. 2 (a) Mercury concentrations ($\mu mol \cdot g^{-1}$ DW) in roots and shoots, and (n = 4) **(b)** chlorophyll fluorescence parameters in wild type (Col-0), *cad2-1*, *pad2-1*, *rax1-1* and *cad1-3 Arabidopsis thaliana* treated with 0 and 3 μM Hg for 72 h: PSII efficiency (Φ_{PSII}), photochemical quenching (q_P) and non-photochemical quenching (NPQ) (n = 8). Different letters denote significant differences at $p<0.05$

Fig. 3 (a) Glutathione reductase (GR) *in gel* activity, **(b)** γ–glutamylcysteine synthetase (γECS) and glutathione reductase (GR) immunodetection in wild type (Col-0), *cad2-1*, *pad2-1*, *rax1-1* and *cad1-3 Arabidopsis* treated with 0 (control) and 3 μM Hg for 72 h. Coomassie-blue staining was used to ensure sample equivalent protein loading. Numbers represent the fold-change relative to the control Col-0, with asterisks marking decreases and decreases ≥ 20%. **(c)** Confocal fluorescence microscopy of *Arabidopsis* Col-0 and *pad2-1* seedling roots treated for 30 min with 0 (control) and 3 μM Hg (two specimens for comparison) to show oxidative stress (H_2DCFDA) induction (green, yellow arrowheads), counterstained with IP to visualise cell walls and detect necrotic cells (red; pink arrowheads).

Fig. 4. PCs and Hg-PC complexes detected by HPLC-ESI-MS(TOF). **(a)** Examples of free PCs and Hg-PCs found in shoots and roots of Col-0 plants exposed to 3 μM Hg for 72 h. Chromatographs and characteristic MS spectra of several molecular ions are shown (in negative mode). **(b)** Summary table describing the different molecular ions of biothiol ligands and Hg-PC complexes detected in shoots and roots of all *Arabidopsis* genotypes treated with 3 μM Hg for 72 h. HPLC-ESI-MS(TOF) was carried out in negative and positive modes, and major detected molecular ions (*m/z*) are shown.

Fig. 5 HPLC-ESI-MS(TOF) analysis of PC and Hg–biothiol complexes in *Arabidopsis* Col-0 xylem sap. **(a)** Chromatographic profile of reduced PC_2, oxidized (PC_2oxd), and $HgPC_2$ detected in the xylem samples (in negative mode). **(b)** $[HgPC_2+H]^+$ Molecular ion distribution (in *m/z*) compared with the theoretical one and a standard complex, prepared by mixing PC_2:$HgCl_2$ at 10:10 μM ratio (in positive mode). **(c)** and **(d)** MS^2 and MS^3 fragmentation profiles of $[HgPC_2+H]^+$, compared to those obtained using a standard PC_2:$HgCl_2$ mixture (insets), all in positive mode.

Fig. 6. Shoot transcriptional qRT-PCR profile of selected genes related to sulphur metabolism, using Col-0, *cad2-1*, *pad2-1*, *rax1-1* and *cad1-3 Arabidopsis* treated with 0 or 3 µM Hg for 72 h. Values are presented as log_2-fold change of Hg-treated plants relative to control plants of each genotype. Statistical differences with Col-0 (at $p < 0.05$) are represented as red and green boxes for over- and down-regulated genes, respectively. Grey boxes indicate no statistical differences. Data of genes encoding transcription factors ( ) are shown in the inset box ( ). Light blue boxes also highlight genes differentially expressed. See quantitative values and statistics in Supplementary Table S4.

Fig. 7. Root transcriptional qRT-PCR profile of selected genes related to sulphur metabolism in Col-0, *cad2-1*, *pad2-1*, *rax1-1* and *cad1-3 Arabidopsis* treated with 0 or 3 µM Hg for 72 h. Values are presented as log_2-fold change of Hg-treated plants relative to control plants of each genotype. Statistically down-regulated genes when compared to Col-0 (at $p < 0.05$) are represented as green boxes, whereas grey boxes indicate no statistical difference. Data of genes encoding transcription factors ( ) are shown in the inset box ( ). Light blue boxes highlight genes differentially expressed. See quantitative values and statistics in Supplementary Table S5.

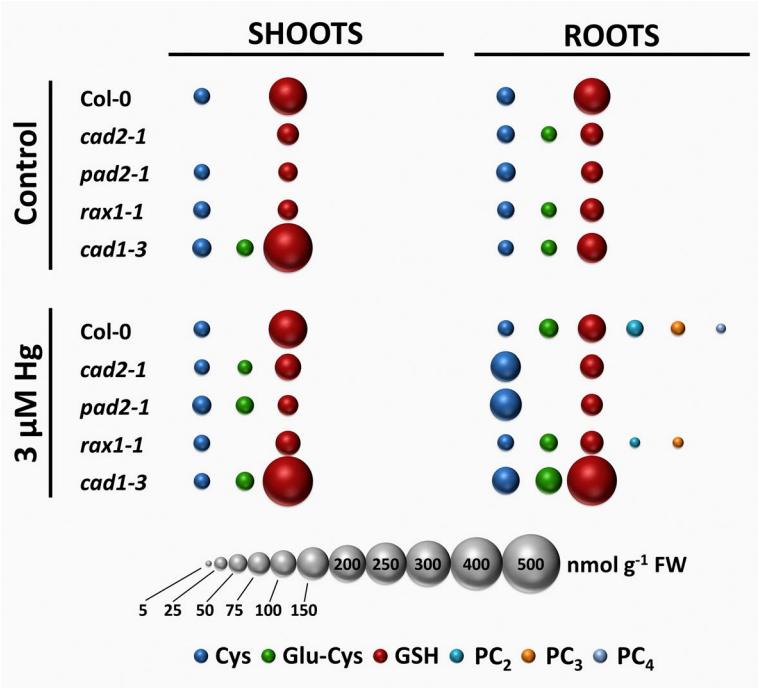
SHOOTS
ROOTS
Control
Col-0
cad2-1
pad2-1
rax1-1
cad1-3
3 µM Hg
Col-0
cad2-1
pad2-1
rax1-1
cad1-3
5
25
50
75
100
150
200
250
300
400
500
nmol g-1 FW
Cys
Glu-Cys
GSH
PC2
PC3
PC4

FIG 1

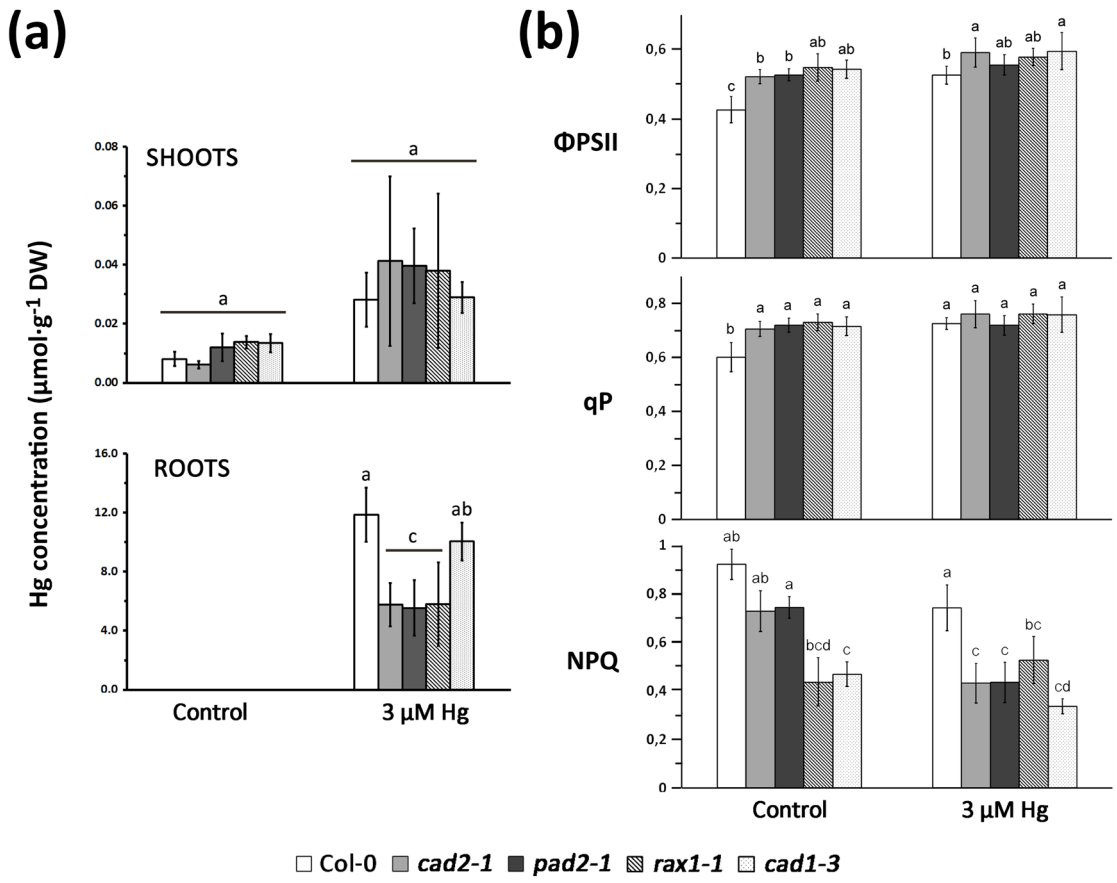
(a)
SHOOTS
ROOTS
Hg concentration (µmol·g-1 DW)
Control
3 µM Hg
(b)
ΦPSII
qP
NPQ
Control
3 µM Hg
Col-0
cad2-1
pad2-1
rax1-1
cad1-3

FIG 2

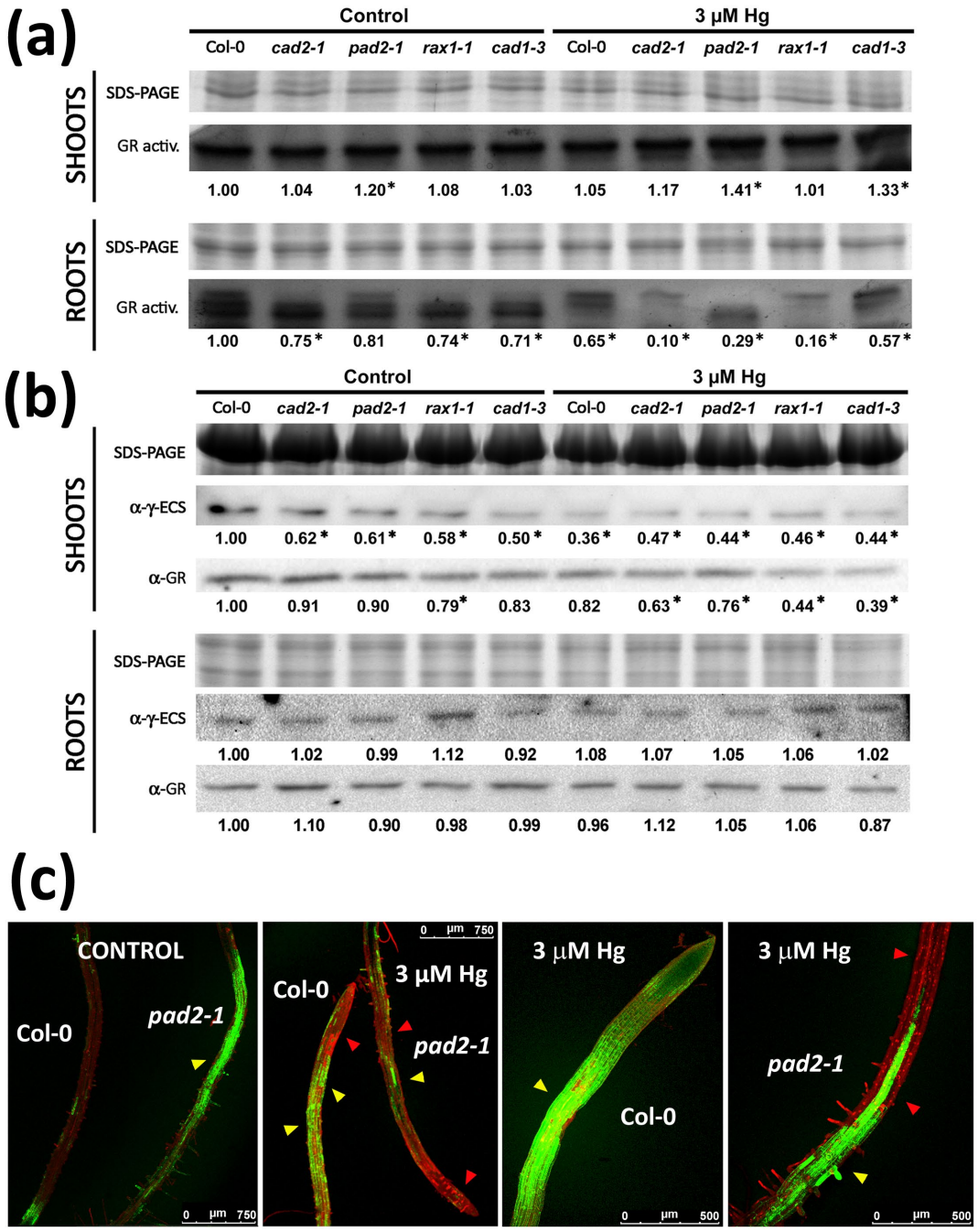
(a)
Control
3 µM Hg
Col-0 cad2-1 pad2-1 rax1-1 cad1-3 Col-0 cad2-1 pad2-1 rax1-1 cad1-3
SHOOTS
SDS-PAGE
GR activ.
1.00 1.04 1.20* 1.08 1.03 1.05 1.17 1.41* 1.01 1.33*
ROOTS
SDS-PAGE
GR activ.
1.00 0.75* 0.81 0.74* 0.71* 0.65* 0.10* 0.29* 0.16* 0.57*
(b)
Control
3 µM Hg
Col-0 cad2-1 pad2-1 rax1-1 cad1-3 Col-0 cad2-1 pad2-1 rax1-1 cad1-3
SHOOTS
SDS-PAGE
α-γ-ECS
1.00 0.62* 0.61* 0.58* 0.50* 0.36* 0.47* 0.44* 0.46* 0.44*
α-GR
1.00 0.91 0.90 0.79* 0.83 0.82 0.63* 0.76* 0.44* 0.39*
ROOTS
SDS-PAGE
α-γ-ECS
1.00 1.02 0.99 1.12 0.92 1.08 1.07 1.05 1.06 1.02
α-GR
1.00 1.10 0.90 0.98 0.99 0.96 1.12 1.05 1.06 0.87
(c)
CONTROL
Col-0
pad2-1
0 µm 750
Col-0
3 µM Hg
pad2-1
0 µm 750
3 µM Hg
Col-0
0 µm 500
3 µM Hg
pad2-1
0 µm 500

FIG 3

(a)

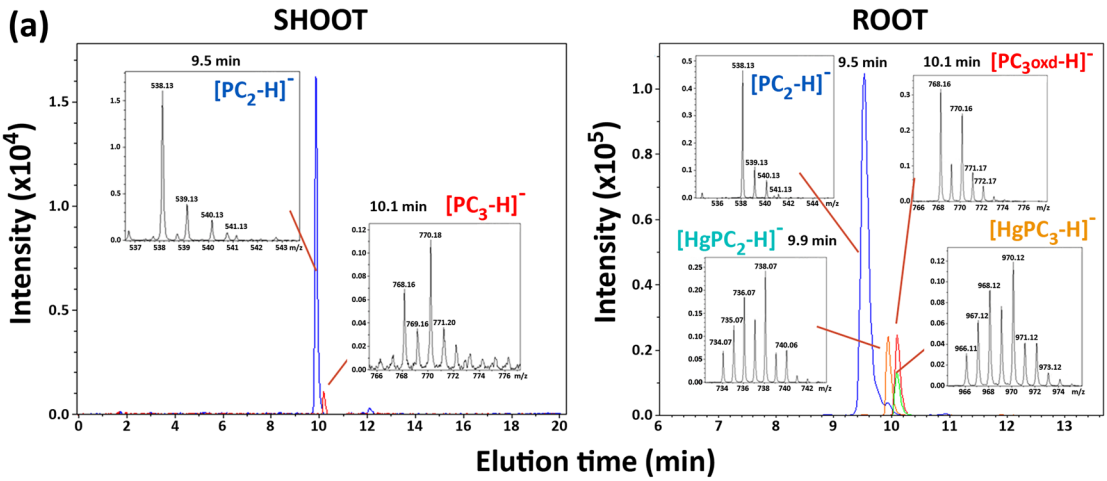

(b)

	Mol. ion	m/z	SHOOTS					ROOTS				
	Genotypes:		Col-0	*cad2-1*	*pad2-1*	*rax1-1*	*cad1-3*	Col-0	*cad2-1*	*pad2-1*	*rax1-1*	*cad1-3*
LIGANDS	$[GSH+H]^+$	308.1										
	$[GSSG+H]^+$	613.3										
	$[PC_2-H]^-$	538.1										
	$[PC_2oxd-H]^-$	536.1										
	$[PC_2+Na-H]^-$	560.1										
	$[PC_3-H]^-$	770.2										
	$[PC_3oxd-H]^-$	768.2										
	$[PC_3+Na-H]^-$	792.2										
COMPLEXES	$[HgPC_2-H]^-$	738.1										
	$[HgPC_2+Na-H]^-$	760.1										
	$[HgPC_3-H]^-$	970.1										
	$[HgPC_3+Na-H]^-$	992.1										

FIG 4

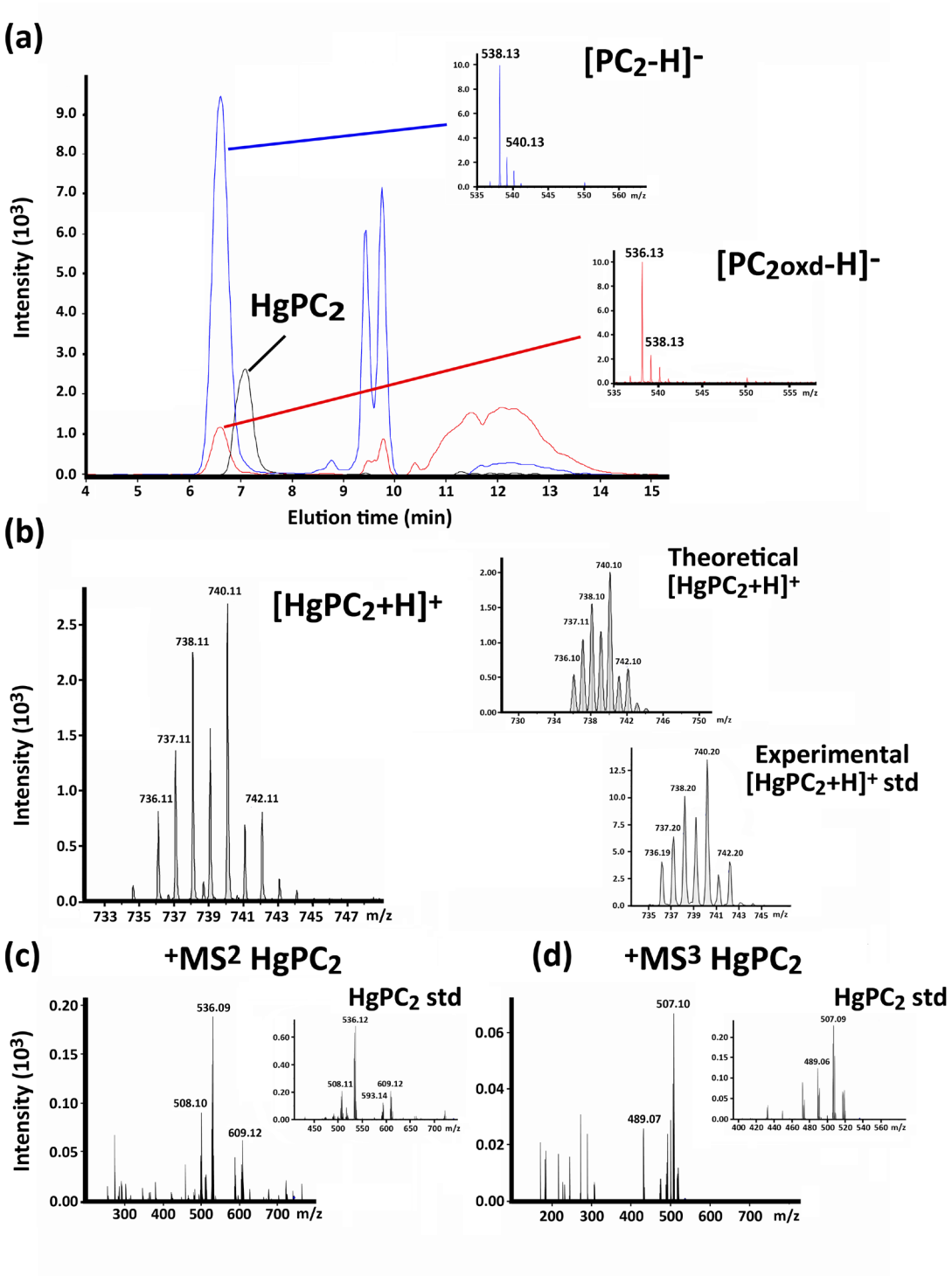
(a)
[PC2-H]-
538.13
540.13
[PC2oxd-H]-
536.13
538.13
HgPC2
Intensity (10³)
Elution time (min)
(b)
[HgPC2+H]+
740.11
738.11
737.11
736.11
742.11
Theoretical
[HgPC2+H]+
740.10
738.10
737.11
736.10
742.10
Experimental
[HgPC2+H]+ std
740.20
738.20
737.20
736.19
742.20
m/z
(c)
+MS2 HgPC2
HgPC2 std
536.09
508.10
609.12
536.12
508.11
609.12
593.14
(d)
+MS3 HgPC2
HgPC2 std
507.10
489.07
507.09
489.06

FIG 5

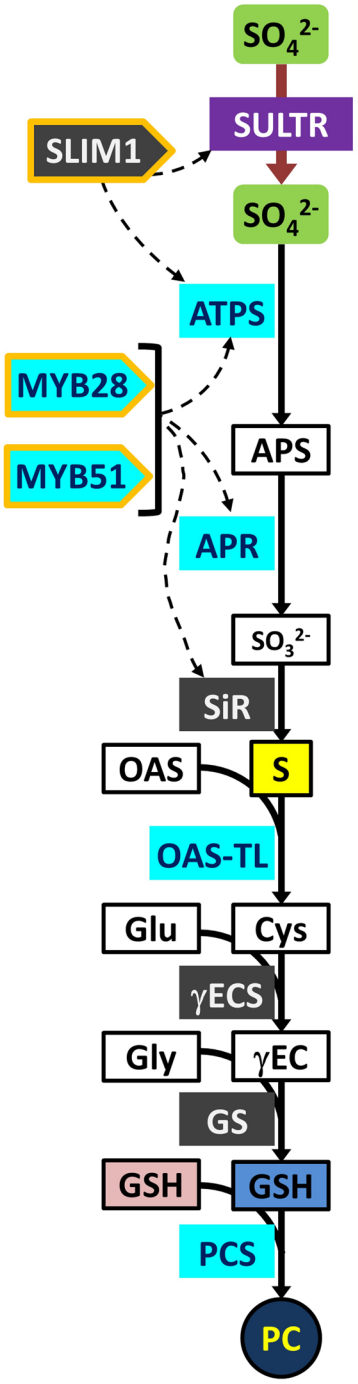

	Col-0	*cad2-1*	*pad2-1*	*rax1-1*	*cad1-3*
MYB28	0,55	1,54	2,26	0,79	0,92
MYB51	0,02	-0,84	-0,06	-1,60	-0,26

SULTR1;2	-3,04	2,57	0,04	4,07	1,88
SULTR3;5	0,20	0,01	1,24	0,40	0,37

ATPS3	-1.27	-0.45	-0.20	-0.49	-0.37
ATPS4	0.14	-0.02	1.04	-1.06	-0.38

APR1	-1.56	0.01	1.37	2.26	1.42
APR2	-0.49	-0.12	1.06	1.30	1.58
APR3	-1.45	0.27	0.59	1.47	0.67

OAS-TL A	-0.21	-1.05	-0.47	-0.72	-0.85
OAS-TL B	-0.51	-0.42	-1.15	-0.81	-0.94

PCS1	-0.21	-0.46	-1.47	-0.96	-0.18
PCS2	-0.02	-0.56	-2.96	-1.36	-2.19

FIG 6

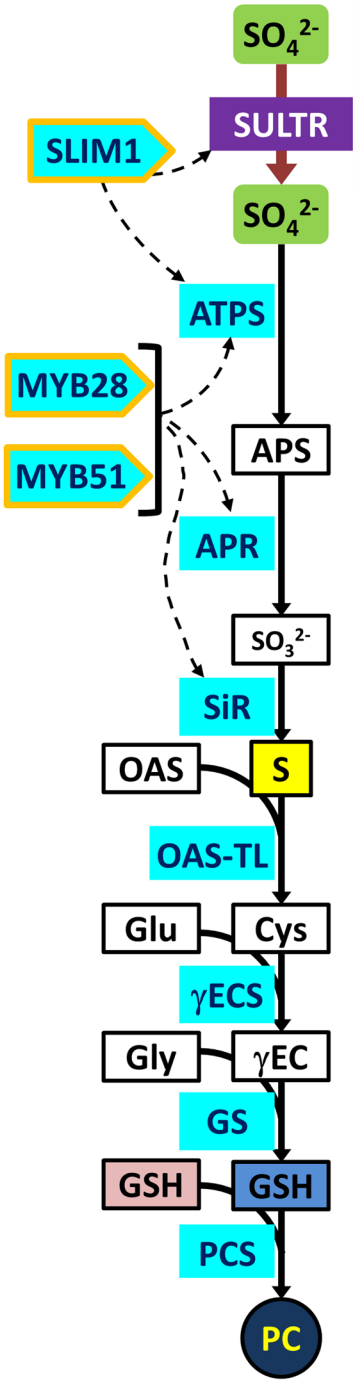

	Col-0	*cad2-1*	*pad2-1*	*rax1-1*	*cad1-3*
SLIM1	-0.48	-1.22	-1.01	-1.67	-1.77
MYB28	-0.63	-1.20	-0.49	-0.67	-1.62
MYB51	-0.49	-1.36	-1.24	-2.72	-4.17
SULTR1;2	-1.87	-2.51	-0.59	-2.41	-2.02
SULTR2;1	0.49	0.49	-0.01	-1.84	-1.84
SULTR3;5	-1.22	-2.00	-1.33	-1.54	-2.22
ATPS1	0.33	-0.87	-0.30	-0.70	-1.51
ATPS3	-0.78	-0.13	0.48	-2.05	-3.78
ATPS4	0.00	-1.47	-0.79	0.29	-0.26
APR2	-0.99	-0.99	-0.69	-0.68	0.26
APR3	-1.06	-0.64	-0.53	-1.69	-0.33
SiR	-0.67	-1.04	-1.52	-0.98	-1.22
OAS-TL B	0.66	-0.77	-2.18	-0.47	-1.31
OAS-TL C	0.35	0.03	0.30	-0.49	-1.20
γECS	-0.69	0.13	0.32	-1.03	-1.17
GS	-0.33	-0.81	-0.09	-0.43	-1.70
PCS1	-0.33	-0.87	0.26	-1.22	-2.74
PCS2	0.08	0.36	0.28	-0.10	-1.11

FIG 7